Cell

Argonaute Divides Its RNA Guide into Domains with Distinct Functions and RNA-Binding Properties

Liang Meng Wee,[1] C. Fabián Flores-Jasso,[1] William E. Salomon,[1] and Phillip D. Zamore[1,*]
[1]Department of Biochemistry and Molecular Pharmacology and Howard Hughes Medical Institute, University of Massachusetts Medical School, Worcester, MA 01605, USA
*Correspondence: phillip.zamore@umassmed.edu
http://dx.doi.org/10.1016/j.cell.2012.10.036

SUMMARY

MicroRNAs (miRNAs) and small interfering RNAs (siRNAs) guide Argonaute proteins to silence mRNA expression. Argonaute binding alters the properties of an RNA guide, creating functional domains. We show that the domains established by Argonaute—the anchor, seed, central, 3′ supplementary, and tail regions—have distinct biochemical properties that explain the differences between how animal miRNAs and siRNAs bind their targets. Extensive complementarity between an siRNA and its target slows the rate at which fly Argonaute2 (Ago2) binds to and dissociates from the target. Highlighting its role in antiviral defense, fly Ago2 dissociates so slowly from extensively complementary target RNAs that essentially every fully paired target is cleaved. Conversely, mouse AGO2, which mainly mediates miRNA-directed repression, dissociates rapidly and with similar rates for fully paired and seed-matched targets. Our data narrow the range of biochemically reasonable models for how Argonaute-bound siRNAs and miRNAs find, bind, and regulate their targets.

INTRODUCTION

Biochemical, computational, and structural studies suggest that Argonaute proteins divide their microRNA (miRNA) or small interfering RNA (siRNA) guides into functionally distinct domains. The most important domain is the seed sequence, which comprises guide nucleotides 2–7 or 2–8 (g2–g8; Lewis et al., 2005; Lewis et al., 2003; Grimson et al., 2007; Doench and Sharp, 2004). Argonaute proteins create the seed by displaying its nucleotides in a prehelical structure that lowers the entropic barrier to target binding (Ma et al., 2005; Parker et al., 2005; Wang et al., 2008a; Parker et al., 2009; Elkayam et al., 2012; Nakanishi et al., 2012; Schirle and MacRae, 2012). The seed sequence is the primary determinant of binding specificity for both miRNAs and siRNAs (Wightman et al., 1993; Lai and Posakony, 1998; Lai, 2002; Haley and Zamore, 2004; Brennecke et al., 2005; Krek et al., 2005; Lim et al., 2005).

In the RNAi pathway, siRNAs direct Argonaute proteins to cleave complementary target RNAs at the phosphodiester bond linking target nucleotide t10 to t11 (i.e., the nucleotides paired to g10 and g11; Elbashir et al., 2001). In addition to seed pairing, target cleavage requires guide:target base pairing in this central region and the adjacent 3′ nucleotides (Ding et al., 2003; Haley and Zamore, 2004; Martinez and Tuschl, 2004; Schwarz et al., 2006). Unlike siRNAs, animal miRNAs rarely pair extensively with their targets (Bartel, 2009), although for some miRNAs, base pairs 3′ to the center of the miRNA supplement the seed sequence (Wightman et al., 1993; Lai and Posakony, 1998; Brennecke et al., 2005; Friedman et al., 2009). In mammals, ~5% of evolutionarily conserved seed-matching miRNA-binding sites have been estimated to contain such 3′ supplementary pairing (Friedman et al., 2009). How this 3′ supplementary region physically contributes to target recognition remains to be established.

Structures of achaeal, eubacterial, yeast, and human Argonaute proteins suggest that the fundamental properties of Argonautes are conserved (Song et al., 2004; Rivas et al., 2005; Yuan et al., 2005; Wang et al., 2008a, 2009; Elkayam et al., 2012; Nakanishi et al., 2012; Schirle and MacRae, 2012). To define the biochemical properties of this class of small RNA-binding proteins, we used *Drosophila melanogaster* Ago2 and *Mus musculus* AGO2 as models. We find that Argonaute divides the small RNA guide into domains—the anchor, seed, central, 3′ supplementary and tail regions—with distinct biochemical properties that explain the differences between how animal miRNAs and siRNAs bind their target mRNAs. Extensive complementarity between an siRNA and its target slows the rate at which fly Ago2 forms a catalytically competent complex and the rate at which it dissociates from an mRNA. In fact, siRNAs tether Argonaute to a highly complementary target so well that nearly all binding events end with cleavage rather than target dissociation. In contrast, Ago2-bound miRNAs paired through the seed sequence bind ≥4-fold more rapidly and dissociate 500-fold more quickly than a cleavage-directing siRNA. Both seed-matched and fully paired small RNAs bound to mouse AGO2 associate with and dissociate from a target RNA at similar rates.

RESULTS

To determine how siRNA:target pairing affects Ago2 function, we systematically altered the sequence of an siRNA whose

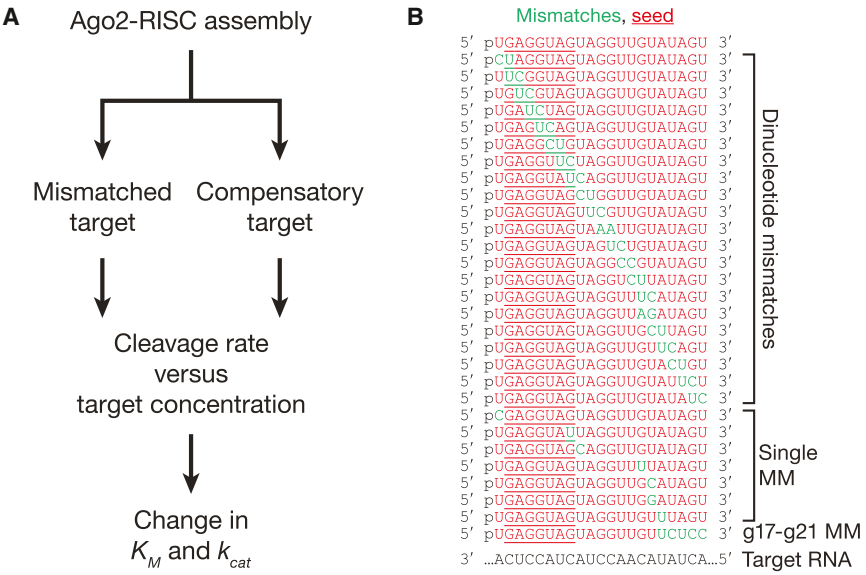

Figure 1. *Drosophila* Ago2 Divides an siRNA into Functional Domains

(A) Kinetic analysis scheme.

(B) siRNAs (red) were used with a single-target RNA to examine the effect of mismatches (green) on target cleavage.

(C and D) A fully complementary target analyzed in parallel for each siRNA was used to calculate the change (mismatched target/fully complementary target) in K_M (C) and k_{cat} (D). Mismatched bases are indicated in boxes. Gray, mismatches that disrupt seed pairing. Data are mean ± SD for ≥ three independent experiments. No cleavage was detected for g11g12 dinucleotide mutations (AA, UU, UA, and UC) or a UCU trinucleotide mutation at g15–g17.

See also Figures S1, S2, and S3 and Tables S1 and S2.

guide strand corresponds to the *let-7* miRNA. We measured the rate of cleavage of a target RNA that was fully complementary to *let-7* for 45 variants of the siRNA. (Figure S1 available online). The use of a common target eliminated the influence on Ago2 activity of target site accessibility (Brown et al., 2005; Ameres et al., 2007; Long et al., 2007; Tafer et al., 2008).

Of 26 overlapping dinucleotide mismatches, 22 reduced the rate of target cleavage by *Drosophila* Ago2 (Figure S1). To understand why some mismatches were tolerated but others were not, we determined the Michaelis-Menten parameters, K_M and k_{cat}, for 59 siRNA:target combinations comprising seven single-nucleotide mismatches, 21 dinucleotide mismatches, a contiguous g17–g21 mismatch, and 30 fully complementary siRNA:target pairs (Figures 1A and 1B and Table S1). Each siRNA was assembled into Ago2-RNA-induced silencing complex (RISC) in *Drosophila* embryo lysate. Half the assembly reaction was used to measure the initial rates of cleavage for a mismatched target and half for a fully complementary target (Figures 1A and S2). Because the RISC concentration was identical for the two targets, the change in k_{cat} attributable to the mismatches corresponded to mismatched V_{max}/fully complementary V_{max}; similarly, the change in K_M equaled mismatched K_M/fully complementary K_M.

A g1 Mismatch Does Not Alter K_M or k_{cat}

In early studies of fly Ago2, a mismatch between siRNA nucleotide g1 and the corresponding t1 position of its target did not impair target cleavage (Haley and Zamore, 2004). Subsequent studies of archaeal (Ma et al., 2005; Parker et al., 2005) and eubacterial (Wang et al., 2008a, 2008b, 2009) Argonautes revealed that binding of the siRNA 5′ phosphate to Argonaute forces the first nucleotide to be unpaired (Ma et al., 2005; Parker

et al., 2005; Wang et al., 2008b). Consistent with these findings, a g1C:t1A mismatch had no detectable effect on the K_M or k_{cat} of fly Ago2 (Figures 1C and 1D).

The Seed Sequence Behaves Like a Small Helix

Seed sequence mismatches increased K_M (Figure 1C). The effect of mismatches on K_M was not constant across the seed (Figure 1C); mismatches at the center of the seed (g4g5) increased K_M 82-fold, whereas the flanking dinucleotide mismatches (g2g3; g3g4; g5g6; and g6g7) increased K_M 11- to 27-fold. These data suggest that base pairs g4:t4 and g5:t5 lie at the center of a 6 or 7 nucleotide RNA helix because central mismatches should disrupt coaxial stacking more than mismatches closer to the ends of the helix. Dinucleotide and single mismatches at the seed periphery (g1g2; g7g8 and g8) had the smallest effect, increasing K_M 1.5- to 3.5-fold. The small effect of peripheral seed mismatches helps explain how miRNAs can regulate their targets through some imperfectly seed-matching sites (Ha et al., 1996; Yekta et al., 2004) and through an "offset 6-mer seed," in which seed pairing begins at g3 and extends to g8 (Friedman et al., 2009).

Dinucleotide mismatches in the seed were generally accompanied by a small increase in k_{cat}; central mismatches caused the greatest effect (e.g., 2.8-fold for a g4g5:t4t5 mismatch). Thus, seed mismatches decreased target binding but enhanced enzyme turnover, perhaps by accelerating release of the 3′ fragment of the cleaved target (Figure 1D).

Central Mismatches Perturb k_{cat}

Target cleavage requires that the center of the siRNA pair with its substrate (Elbashir et al., 2001; Holen et al., 2002; Amarzguioui et al., 2003; Ding et al., 2003; Haley and Zamore, 2004). Central pairing positions the scissile phosphate of the target near the amino acid side chains that catalyze cleavage (Ma et al., 2005; Parker et al., 2005). Structures of eubacterial Argonaute bound to a DNA guide paired to RNA targets of different lengths suggest that base pairing at the center of the guide moves the three catalytic residues—and, presumably, the Mg^{2+} they bind—closer to the target (Wang et al., 2009). For yeast Argonaute, the rearrangement brings a fourth conserved glutamate into the catalytic site (Nakanishi et al., 2012). For fly Ago2, mismatches spanning g8 to g12 all reduced target cleavage, albeit to widely varying extents (Figures 1D and S1).

Although single-nucleotide mismatches at g8 or g9 had little effect on K_M or k_{cat}, a g8g9 dinucleotide mismatch reduced k_{cat} by 93-fold (Figure 1D). Dinucleotide mismatches at g8g9 had a similar effect on k_{cat} for a *luciferase*-targeting siRNA (Figures S3A–S3C; p value = 1.7×10^{-8}; two-tailed, unpaired Student's t test). The effects on k_{cat} of dinucleotide mismatches at g9g10 (5.0-fold reduction) and g10g11 (16-fold reduction) were more modest (Figure 1D). We saw no target cleavage for a g11g12 dinucleotide mismatch. (Our assay can detect ~500-fold decrease in k_{cat}.) Mismatches at positions g9g10 or g10g11 did not alter K_M. Our data support the idea that central pairing enables Ago2 to achieve a catalytically competent conformation but contributes little to target binding.

Only a Subset of 3′ Base Pairs Contribute to K_M or k_{cat}

Target pairing 3′ to the center of the small RNA has been proposed to enable Argonaute to achieve a catalytically competent conformation (Haley and Zamore, 2004). Consistent with this view, a dinucleotide mismatch at g12g13 reduced k_{cat} 16-fold, although dinucleotide mismatches at g14g15, g15g16, g16g17, or g17g18, as well as a single mismatch at g15, reduced k_{cat} 1.5- to 9.4-fold (Figure 1D). Similarly, a g15g16 dinucleotide mismatch in a *luciferase*-targeting siRNA decreased k_{cat} 7.6-fold, compared to a fully matched target RNA (Figure S3). A dinucleotide mismatch at g13g14 however, did not decrease k_{cat} (Figure 1D). We do not know why this dinucleotide mismatch alone among the six had no detectable effect. We note that this atypical dinucleotide mismatch (CC:AA) lies between a GG:CC (g11g12) dinucleotide and G:C pair (g15). These flanking base pairs may mitigate the helical disruption caused by the intervening pyrimidine:purine dinucleotide mismatch.

The effect on K_M of dinucleotide mismatches from g12 to g17 was qualitatively similar to mismatches in the seed sequence (Figure 1C). Pairing to miRNA bases g13–g16 ("3′ supplementary base pairing") is a computational hallmark of a high confidence miRNA-binding site (Brennecke et al., 2005; Grimson et al., 2007; Bartel, 2009; Friedman et al., 2009). We observed a small but significant increased in K_M for dinucleotide mismatches at g13g14 (3.6-fold, p value = 0.022), g14g15 (4.2-fold, p value = 0.017) and g15g16 (3- to 4-fold, p value = 6.6×10^{-3}) and for a single-nucleotide mismatch at g16:t16 (3.4-fold, p value = 4.7×10^{-3}; Figure 1C and Tables S1 and S2). A g15g16 dinucleotide mismatch also increased the K_M of the *luciferase* siRNA by 12-fold (p value = 7.6×10^{-4}; Figure S3B). Notably, the 7 nt seed of this siRNA is predicted to pair more weakly with its target ($\Delta G_{seed(25°C)} = -7.7$ kcal mol^{-1}) than the seed of the *let-7* siRNA ($\Delta G_{seed(25°C)} = -11.2$ kcal mol^{-1}). Weaker seed pairing likely makes 3′ supplementary base pairing more important (Brennecke et al., 2005).

Mismatches at the center of the g12–g17 region had the greatest effect on K_M, with a g14g15 dinucleotide mismatch increasing K_M 4.2-fold. The g14g15 base pairs probably lie at the center of a small RNA helix, much as the g4g5 base pairs do for the seed.

The siRNA 3′ End Contributes Little to K_M or k_{cat}

The g17:t17 base pair marks the end of the 3′ supplementary binding site: a single-nucleotide mismatch at g17 and dinucleotide mismatches at g18g19 and g19g20 caused no significant change in K_M or k_{cat}. A g17g18 dinucleotide mismatch decreased k_{cat} by 2.2-fold (p value = 0.037), whereas a g17–g21 contiguous mismatch decreased k_{cat} by 1.9-fold (p value = 0.024), but neither had an effect on K_M. In contrast, a trinucleotide mismatch within the 3′ supplementary region (g15–g17) completely inhibited target cleavage (Figures 1C, 1D, and S1).

Notably, a dinucleotide mismatch at g20g21 caused a modest increase in both K_M (1.9-fold, p value = 1.7×10^{-3}) and k_{cat} (1.6-fold, p value = 6.9×10^{-3}), consistent with earlier suggestions that terminal mismatches facilitate product release from plant and animal RISC (Tang et al., 2003; Haley and Zamore, 2004). We conclude that the final four nucleotides of the small

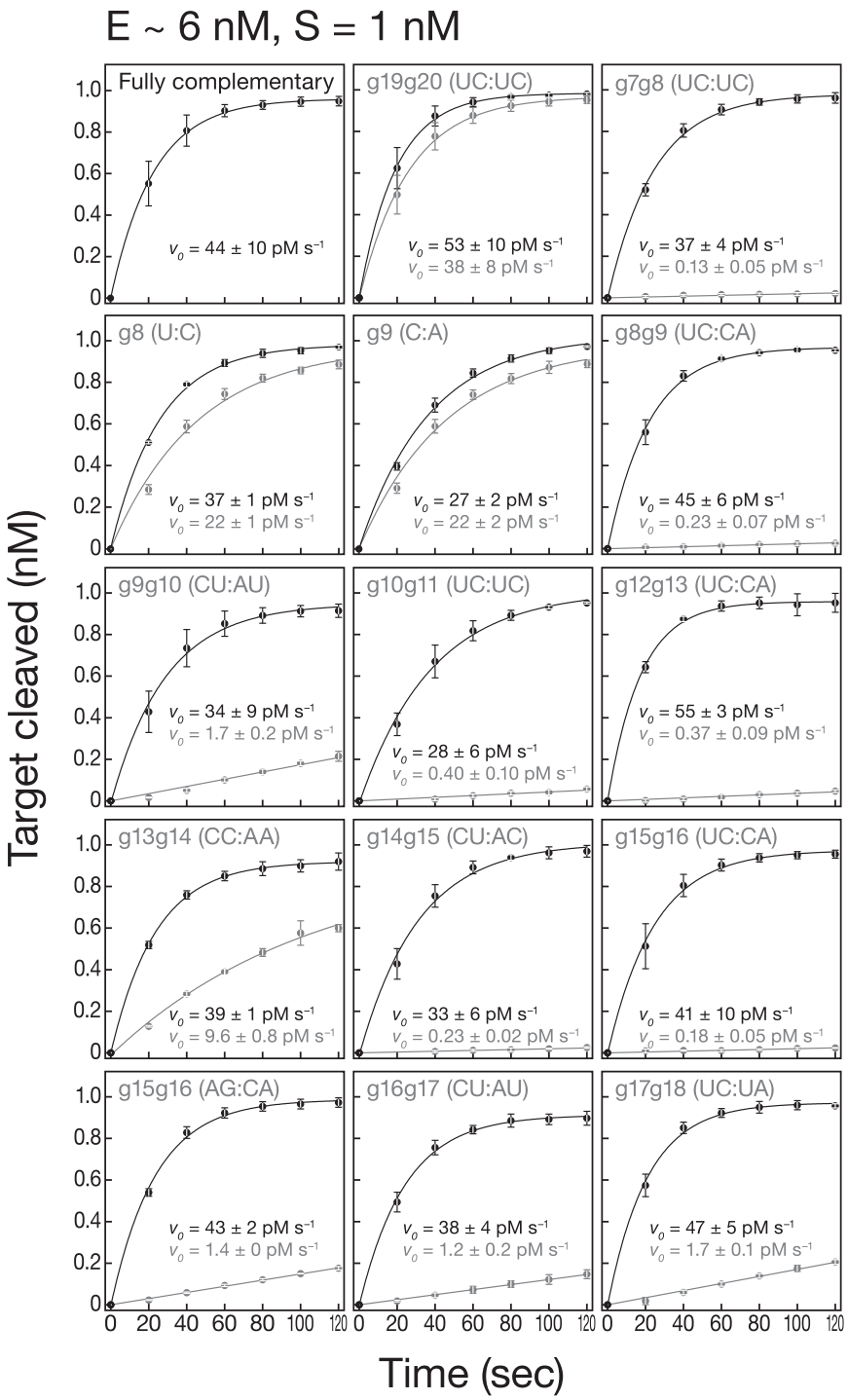

Figure 2. Mismatches that Impair k_{cat} Disrupt Catalysis but Promote Turnover

Target cleavage with [S] < [E]. Initial rates, v_0, for mismatched (gray) and fully complementary targets (black) were determined by fitting the data to a single exponential. Table S1 lists the change in initial rates (mismatched versus fully complementary). Data are mean ± SD for ≥ three independent experiments.

RNA guide—the "tail"—form base pairs only after the target RNA is cleaved.

Mismatches that Reduce k_{cat} Reflect a Defect in Catalysis

Mismatches that reduce k_{cat} could reflect a defect in catalysis, product release, or regeneration of RISC to an active state. For these mismatches, we measured the initial rate of target cleavage (v_0) under conditions of enzyme excess. When [E] > [S], v_0 is largely uninfluenced by product release or enzyme regeneration because most RISCs cleave just a single molecule of target.

All mismatches that reduced the multiple turnover cleavage rate also decreased the rate when [E] > [S] (Figure 2 and Table S1). Thus, a defect in the catalytic step suffices to explain the reduced k_{cat}. In fact, the effects of mismatches were greater when [E] > [S] than when [E] << [S], suggesting that the deleterious effect of mismatches on the inherent rate of target cleavage is partially offset by a favorable effect of mismatches on steps present only when each RISC catalyzes many successive rounds of target cleavage (Table S1, relative k_{cat}/relative v_0). In other words, mismatches inhibited catalysis but promoted product release or enzyme regeneration. This was most pronounced for mismatches in the seed and 3′ supplementary region (Table S1, relative k_{cat}/relative v_0), favoring the idea that mismatches in these domains promote product release, just as they facilitate the release of miRNA* from pre-Ago1-RISC in flies and humans (Tomari et al., 2007; Kawamata et al., 2009; Yoda et al., 2010).

The Standard Rules for RNA Base Pairing Apply to RISC

Might Ago create a special environment for seed base paring? To test whether the standard rules for RNA base pairing apply, we used the change in K_M between mismatched and fully complementary siRNA:target pairs to calculate the free energy cost of mismatches in the seed. We compared this to the cost predicted by nearest neighbor analysis (Xia et al., 1998).

First, we tested whether nearest neighbor values determined in 1 M sodium (pH 7.0; Schroeder and Turner, 2009), changed in our more physiological conditions (100 mM potassium,

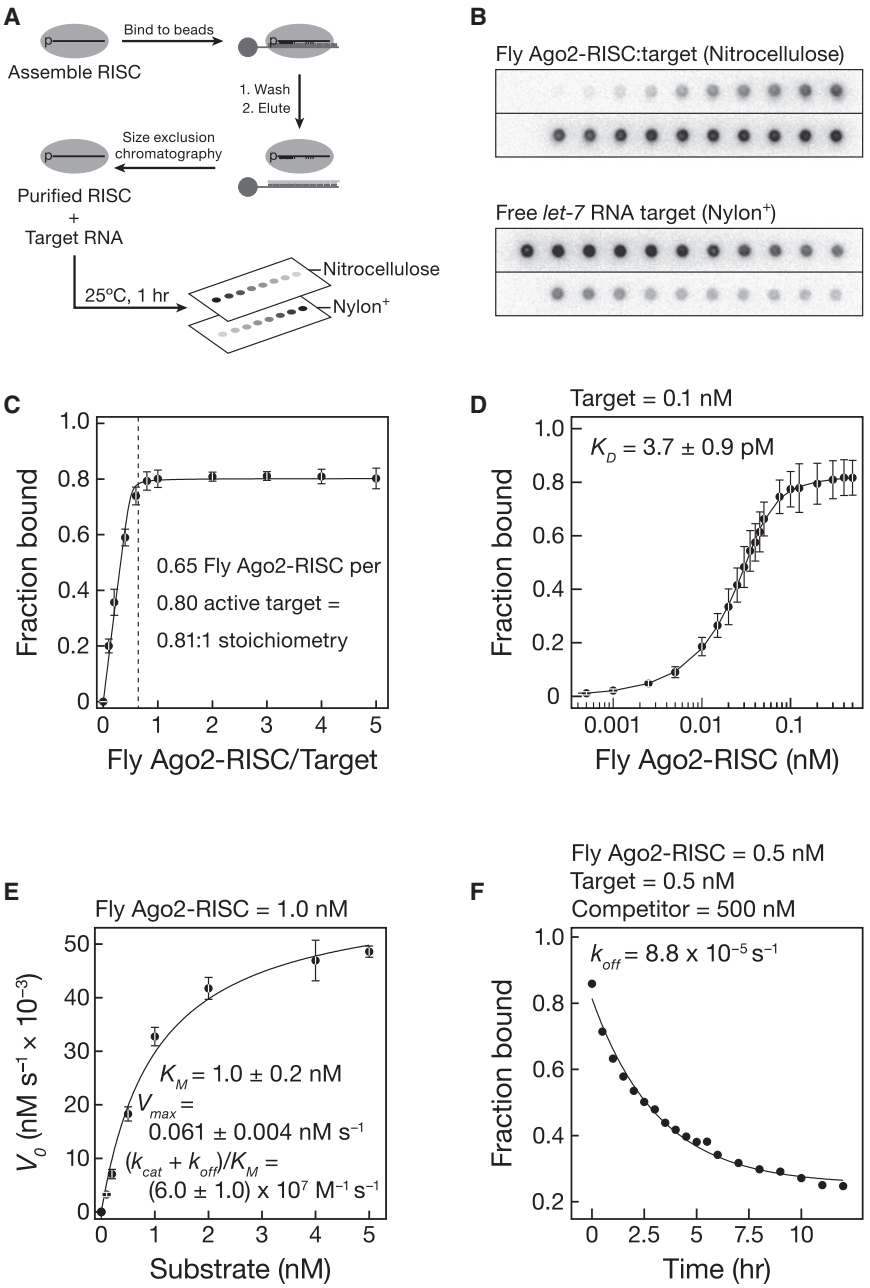

Figure 3. Fly Ago2-RISC Binding

(A) RISC was assembled and then purified with a partially complementary, tethered 2′-*O*-methyl oligonucleotide.

(B) Purified Ago2-RISC was then used in filter-binding assays.

(C) Stoichiometric binding titration of target RNA with increasing amounts of purified fly Ago2-RISC. Data are mean ± SD.

(D) Equilibrium binding assays. Data are mean ± SD for 15 independent experiments with three preparations of fly Ago2-RISC.

(E) Kinetics of purified fly Ago2-RISC with a 29 nt fully complementary target RNA. Data are mean ± SD for three independent experiments.

(F) Dissociation rate for a fully complementary target RNA.

See also Figures S4 and S5, and Table S3.

4 mM magnesium [pH 7.4]). Values obtained in our conditions agreed well with the published data (Figures S4A and S4B and Table S3). Second, an increase in K_M may reflect an increase in k_{cat} because $K_M = (k_{off} + k_{cat})/k_{on}$. For mismatches in the seed and 3′ supplementary regions, we detected no correlated changes between K_M and k_{cat}, justifying our use of the change in K_M as a surrogate for relative K_D.

The free energy cost, $\Delta\Delta G_{25°C}$, calculated from the change in K_M for both seed ($r = 0.93$, p value = 4.1×10^{-4}) and 3′ supplementary ($r = 0.76$, p value = 2.0×10^{-3}) mismatches correlated well with the values predicted by the nearest neighbor values for RNA base pairing (Figures S4C and S4D). Thus, the relative contributions of each base pair in RISC are similar to those in an RNA:RNA duplex.

Ago2 Reduces the Affinity of a Guide RNA for Its Target

A key obstacle to measuring the binding affinity of Ago2-RISC has been the inability to purify Ago2 bound to a single siRNA guide sequence. We recently developed a simple and efficient method for purifying mature RISC assembled in *Drosophila* embryo lysate or mouse embryonic fibroblast S100 lysate (C.F.F.-J. and P.D.Z., unpublished data; Figures 3A and 3B). (Mouse and human AGO2 are 99% identical.) We used nitrocellulose filter binding to measure the binding affinity of both fly Ago2-RISC and mouse AGO2-RISC purified by this procedure (fly, Figures 3, 4, and 5; mouse, Figure 6). RISC concentration was determined by quantitative northern hybridization and pre-steady-state analysis (Figures S5A–S5C). To block cleavage, the target RNA contained a phosphorothioate linkage flanked by 2′-*O*-methyl ribose at positions t10 and t11 (Figures S5D and S5E). Stoichiometric titration showed that 0.81 fly Ago2-RISC and 1.4 mouse AGO2-RISCs bound each molecule of target, consistent with one RISC per target (Figures 3C, 6A, and 6B).

Fly Ago2- and mouse AGO2-RISC bound tightly to a fully complementary RNA (Figures 3D and 6C). Our K_M data and published Argonaute structures (Wang et al., 2009) suggest that 16–17 base pairs form between the guide and the target RNAs, yet the binding affinity of fly Ago2-RISC (K_D = 3.7 ± 0.9 pM, mean ± S.D.; $\Delta G_{25°C}$ ~16 kcal mol^{-1}) and mouse AGO2-RISC (K_D = 20 ± 10 pM, mean ± S.D.; $\Delta G_{25°C}$ ~15 kcal mol^{-1}; see below) for a fully complementary target was comparable to

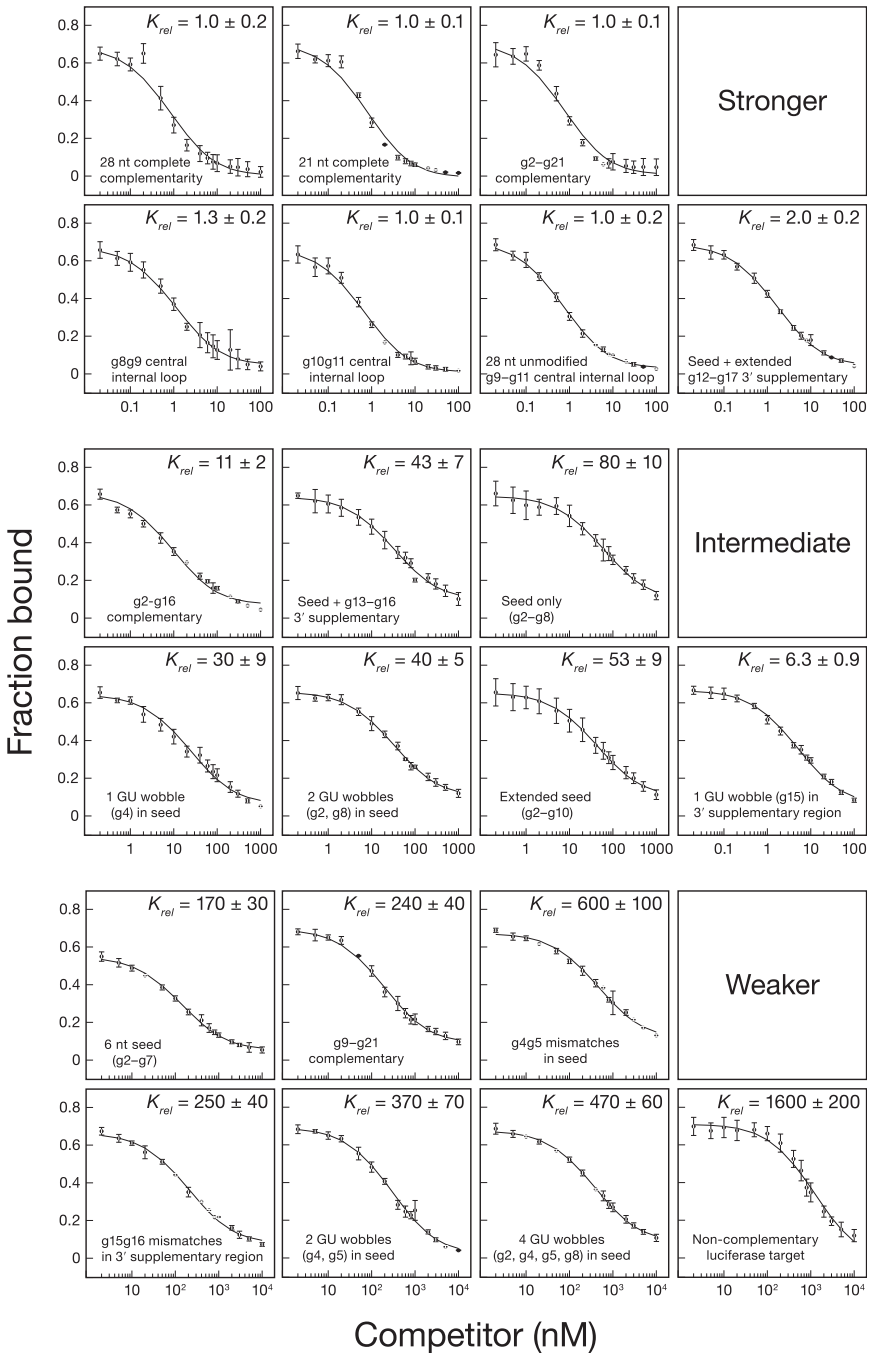

Figure 4. Fly Ago2-RISC Equilibrium Competition

The equilibrium dissociation constant of fly Ago2-RISC for the competitor, relative to that of a fully complementary target, is reported as the mean K_{rel} ± SD for ≥ three independent experiments. See also Table S4.

that of a 10 bp RNA:RNA helix. Thus, Argonaute functions to *weaken* the binding of the 21 nt siRNA to its fully complementary target: without the protein, the siRNA, base paired from positions g2 to g17, is predicted to have a K_D ~3.0 × 10^{-11} pM ($\Delta G_{25°C}$ = −30.7 kcal mol^{-1}). Argonaute raises the K_D of the 16 bp RNA:RNA hybrid by a factor of > 10^{11}.

K_M is not K_D

The K_D measured in our binding assay (3.7 ± 0.9 pM) was ~270-fold smaller than the K_M (1.0 ± 0.2 nM) determined with purified fly Ago2 (Figure 3E). By definition, K_M = (k_{off} + k_{cat})/k_{on}. When k_{cat} << k_{off}, K_M ~K_D. To understand why K_M so dramatically underestimates the affinity of fly Ago2 for a fully complementary target, we measured k_{off} directly (Figure 3F). For fly Ago2-RISC, the dissociation rate constant, k_{off} = 8.8 × 10^{-5} s^{-1}, was much slower than the turnover rate, k_{cat} = 6.1 × 10^{-2} s^{-1}. Consequently, K_M ~k_{cat}/k_{on}. Hence, for fly Ago2-RISC, K_M is not K_D.

In contrast, the K_D for mouse AGO2 (20 ± 10 pM) was only ~5-fold smaller than the K_M (0.10 ± 0.06 nM), because for mouse the dissociation rate (k_{off} = 7.7 × 10^{-4} s^{-1}) is comparable to k_{cat} (8.1 × 10^{-4} s^{-1}; Figures 6C and 6D). For mouse AGO2-RISC, K_M~ K_D.

We used a competition assay to determine the contributions to binding of the anchor, seed, central, 3′ supplementary, and tail regions of the siRNA. For the fully complementary *let-7* target, this assay gave values similar to those measured in the direct binding assay: 10 ± 1 pM (Figure 4 and Table S4) versus 3.7 ± 0.9 pM (Figure 3D) for fly and 36 ± 5 pM (Figure 6E and Table S4) versus 20 ± 10 pM (Figure 6C) for mouse. Binding was specific: a noncomplementary *luciferase* RNA target competed ~1,600-fold less tightly for fly Ago2 (Figure 4) and ~100-fold less efficiently for mouse AGO2 (Figure 6E). Single-stranded sequences flanking the RISC-binding site in a target RNA have been reported to have no effect on the K_M of human AGO2-RISC (Ameres et al., 2007), and we detected no difference in binding between a 28 nt (K_D = 3.9 ± 0.9 pM) and a 21 nt (K_D = 3.6 ± 0.7 pM) competitor for fly Ago2 (Figure 4 and Table S4).

The Fly Ago2 Seed Does Not Tolerate GU Wobble Pairs

GU wobble pairs between miRNAs and their targets have been reported to be tolerated, and some miRNA target prediction algorithms permit GU wobbles even in the seed (John et al., 2004; Miranda et al., 2006; Kertesz et al., 2007). We measured the effect of seed GU wobble pairs on target binding by fly

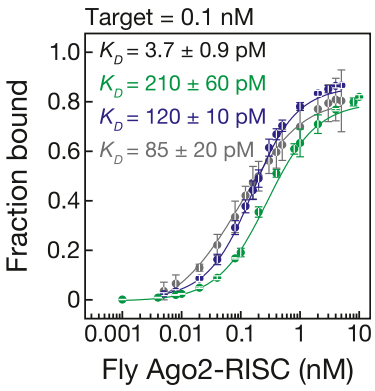

Figure 5. Fly Ago2-RISC Binds Seed-Matched Targets at the Rate of Diffusion

(A) Binding and dissociation was analyzed for target RNAs (left) that were complementary (black) to the entire siRNA (red), the seed (green), the seed plus 3′ supplementary region (blue), or positions g2–g10 (gray). Asterisk, ^{32}P radiolabel; subscript "m", 2′-*O*-methyl ribose; "ps", phosphorothioate linkage.

(B) Dissociation rates for the RNAs in (A). For the dissociation rate curve for the fully complementary RNA, see Figure 3F.

Data are mean ± SD. See also Figure S6.

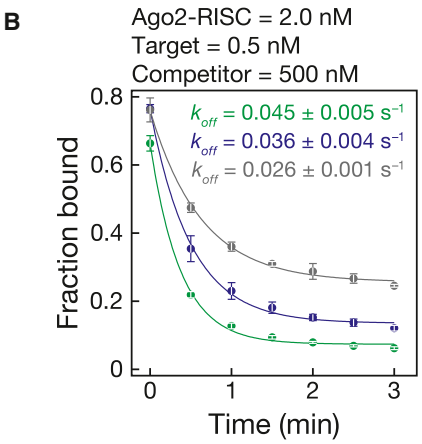

Ago2-RISC (Figure 4). A GU wobble at g4 decreased K_D by 30-fold; two GU wobbles (g2, g8) decrease K_D 40-fold (Figure 4). Two GU wobbles at the center of the seed (g4, g5) reduced binding 370-fold, and four GU wobbles (g2, g4, g5, g8) decreased binding 470-fold. We conclude that GU wobbles behave like mismatches and are not tolerated in the seed. Our data explain earlier reports that GU wobbles interfere with Argonaute function (Doench and Sharp, 2004; Brennecke et al., 2005; Grimson et al., 2007) and suggest that GU pairs in the seed should not be allowed by miRNA target prediction algorithms.

Just Two-Thirds of siRNA Nucleotides Contribute to Binding for Fly Ago2

Mismatches at g1, g8g9, or g10g11 had little or no effect on binding. Likewise, a target lacking phosphorothioate and 2′-*O*-methyl modifications but mismatched with the siRNA from positions g9–g11 bound with an affinity similar to that of the fully complementary, modified RNA (K_{rel} = 1.0–1.3; Figure 4). A target complementary to only siRNA nucleotides g2–g16 bound just 11-fold less tightly than a target with complete, 21 nt complementarity. In contrast, a g4g5 dinucleotide mismatch in the seed weakened binding 600-fold; a g15g16 mismatch in the 3′ supplementary region reduced binding 250-fold (Figure 4).

Thus, more than a third of the nucleotides in an siRNA guide make little or no contribution to target binding. Supporting this view, a target RNA complementary to only g2–g8 (the seed) and g12–g17 (extended 3′ supplementary pairing) bound nearly as tightly as the fully complementary RNA (K_{rel} = 2.0 ± 0.2; Figure 4). Yet, a target complementary only to the seed and the 3′ supplementary region (g2–g8; g13–g16) bound 43-fold less tightly than the fully complementary target; a target complementary only to the seed bound 80 times less tightly. Direct binding measurements yielded essentially the same results as the competition assay (Figure 5A). Although the seed and 3′ supplementary regions supply much of the energy used by RISC to bind targets, nucleotides adjacent to the 3′ supplementary region also contribute to binding for fly Ago2-RISC.

For Fly Ago2-RISC, a 7 nt Seed Binds Better Than a 6-mer

Computational analysis in flies suggested that in the absence of 3′ supplementary pairing, 7 nt (g2–g8) but not 6 nt (g2–g7) seed complementarity can distinguish authentic miRNA-binding sites from chance complementarity (Brennecke et al., 2005), unlike in mammals, where both types of seed-matching sites have predictive power (Lewis et al., 2005). Intriguingly, fly Ago2-RISC bound a 6-mer seed-matching target 2-fold less tightly than the 7-mer seed (Figure 4). Because most miRNAs function through Ago1 in flies, it remains to be tested whether Ago1 behaves similarly.

Mouse AGO2 Is Optimized for miRNA Regulation, Not RNAi

Like fly Ago2, competition assays performed with mouse AGO2-RISC showed that central (g10g11) and terminal mismatches (g20g21) had no detectable effect on binding, whereas g4g5 seed mismatches reduced binding 40-fold (Figure 6E). Surprisingly, g15g16 mismatches did not impair binding for mouse AGO2-RISC (K_{rel} = 1.4 ± 0.6; Figure 6E). Moreover, direct binding assays found no substantive difference in affinity between a seed-matching (K_D = 26 ± 2 pM) and a fully complementary target (20 ± 10 pM; Figure 6C). We did observe a small

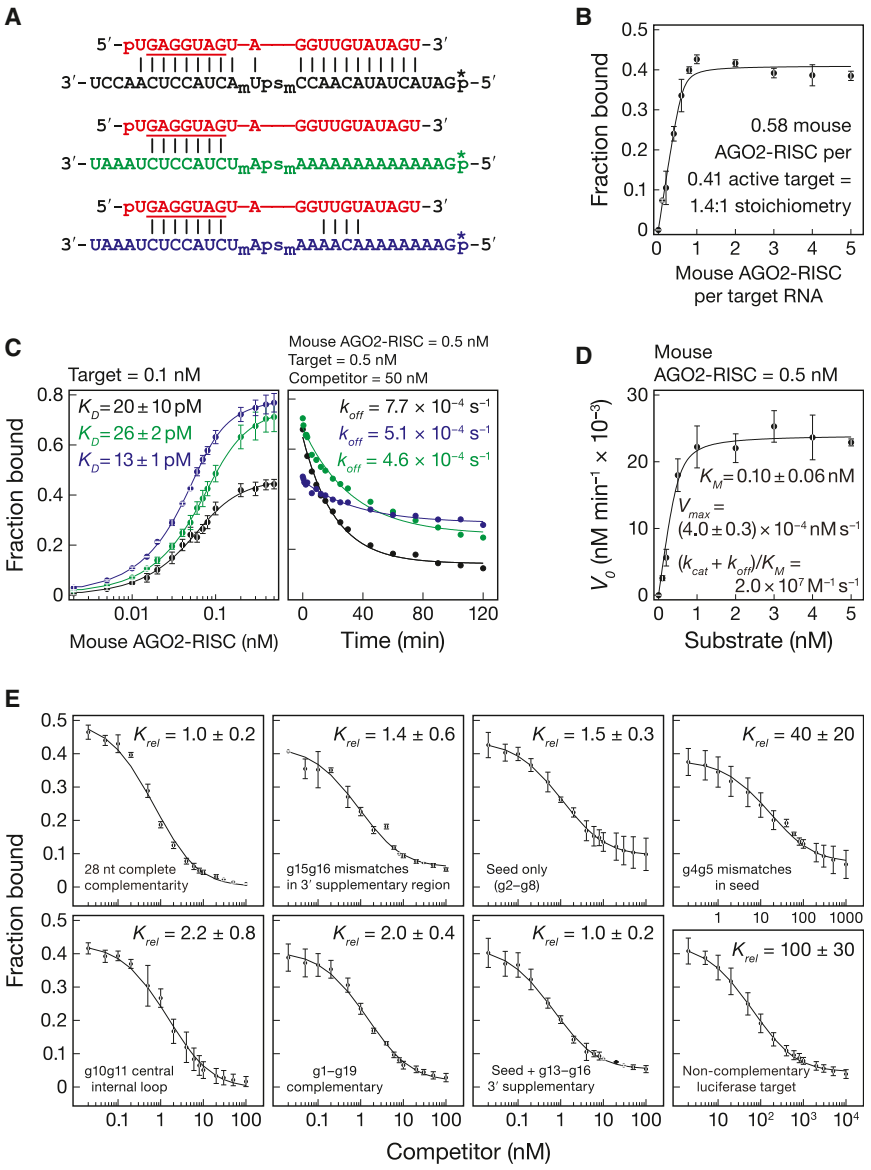

Figure 6. Mouse AGO2-RISC is Specialized for miRNA Regulation

(A) Binding and dissociation analyses for target RNAs that were complementary (black) to the entire siRNA (red), the seed (green), or the seed plus 3′ supplementary region (blue).

(B) Stoichiometric binding titration with increasing amounts of mouse AGO2-RISC.

(C) Equilibrium binding (left) and dissociation assays (right). Data are mean ± SD for ≥ three independent experiments.

(D) Kinetics of purified mouse AGO2-RISC with a 28 nt fully complementary target. Data are mean ± SD for three independent experiments fitted to the quadratic equation for tight binding.

(E) The equilibrium dissociation constant of mouse AGO2-RISC for the competitor, relative to that of a fully complementary target, is reported as the mean K_{rel} ± SD for ≥ three independent experiments.

but significant (p value = 3.2×10^{-4}) increase in affinity for a target with seed and 3′ supplementary pairing (K_D = 13 ± 1 pM), compared to the affinity of a target with seed pairing alone. The modest contribution of the 3′ supplementary region to target binding helps explain why in mammals less than 5% of evolutionarily conserved, predicted miRNA-binding sites include conserved 3′ pairing (Friedman et al., 2009). We conclude that seed complementarity and, to a far lesser extent, 3′ supplementary base pairing, provide all the binding energy tethering mouse AGO2-RISC to its targets. Our data suggest that evolution has optimized mammalian AGO2 for miRNA-based regulation. In contrast, fly Ago2 binds far more tightly to fully complementary targets than to those matching only the seed, as might be expected for an enzyme responsible for binding and destroying viral and transposon transcripts.

Essentially Every Target that is Fully Paired to Fly Ago2-RISC Is Cleaved

To understand the molecular basis for the difference between mouse and fly Ago2-RISC, we measured the rate of dissociation of *let-7*-programmed fly Ago2-RISC for several prototypical RNA targets (Figure 5A).

Fly Ago2-RISC dissociated slowly from a fully complementary target: $k_{off} = 8.8 \times 10^{-5}$ s^{-1}, corresponding to a half-life ($t_{1/2}$) ~2.2 hr (Figure 3F). Given that k_{cat} for *let-7*-programmed fly Ago2-RISC was 6.1×10^{-2} s^{-1} ($t_{1/2}$ ~11 s), essentially every fly Ago2-RISC that binds a target will slice it rather than dissociate from the uncleaved RNA (Figure 3E).

RISC dissociated far more rapidly from targets paired to the seed sequence (g2–g8) or the seed plus the 3′ supplementary region (g13–g16): $k_{off} = 4.5 \times 10^{-2}$ s^{-1} ($t_{1/2}$ ~15 s) for seed-matched and $k_{off} = 3.6 \times 10^{-2}$ s^{-1} ($t_{1/2}$ ~19 s) for seed plus 3′ supplementary pairing (Figure 5B). Such rapid dissociation from partially paired targets may minimize titration of RISC by seed-matching off-targets. Intriguingly, fly Ago2-RISC dissociated more slowly from a target that paired with an extended seed-match (g2–g10; $k_{off} = 2.6 \times 10^{-2}$ s^{-1}, $t_{1/2}$ ~27 s) than from a target complementary to both the seed and 3′ supplementary region (Figure 5B).

Mouse AGO2-RISC Often Dissociates before It Cleaves

Mouse AGO2-RISC dissociated ~90-fold more slowly from a seed-matched target ($k_{off} = 5.1 \times 10^{-4}$ s^{-1}; $t_{1/2}$ ~23 min) than did fly Ago2. Moreover, the mouse AGO2 dissociation rate constants for targets matching the seed, seed plus 3′ supplementary region ($k_{off} = 4.6 \times 10^{-4}$ s^{-1}; $t_{1/2}$~25 min), and the entire RNA guide ($k_{off} = 7.7 \times 10^{-4}$ s^{-1}; $t_{1/2}$ ~15 min) were

quite similar (Figure 6C), consistent with their similar K_D values. Given that the k_{cat} for purified mouse AGO2-RISC was 8.1 × 10^{-4} s^{-1} ($t_{1/2}$ ~14 min; Figure 6D), a fully complementary target is as likely to dissociate as to be cleaved.

Our data also suggest that in both flies and mammals, the typical miRNA:Argonaute complex is in rapid equilibrium between the target-bound and unbound states, explaining why RNA-binding proteins can compete with miRNAs for overlapping binding sites (Bhattacharyya et al., 2006; Huang et al., 2007; Kedde et al., 2007; Elcheva et al., 2009; Takeda et al., 2009; Goswami et al., 2010; Jafarifar et al., 2011; Toledano et al., 2012).

miRNAs in RISC Find Their Targets at Rates that Approach that of Diffusion

We used our experimentally determined K_D and k_{off} to calculate k_{on} (= k_{off} /K_D), the bimolecular association rate constant for RISC binding its target. For both fly and mouse AGO2-RISC, k_{on} for targets matching only the seed and the seed plus the 3′ supplementary region were similar: k_{on} (seed) = 2.1 × 10^8 M^{-1} s^{-1} and k_{on} (seed plus 3′ supplementary) = 3.1 × 10^8 M^{-1} s^{-1} for fly Ago2; k_{on} (seed) = 2.0 × 10^7 M^{-1} s^{-1} and k_{on} (seed plus 3′ supplementary) = 3.6 × 10^7 M^{-1} s^{-1} for mouse AGO2. These rates suggest that miRNA-programmed Argonautes find their target RNAs near the limits of macromolecular diffusion (Hammes and Schimmel, 1970; Berg and von Hippel, 1985).

For fly Ago2-RISC, a dinucleotide mismatch that disrupts seed pairing (g4g5) reduced k_{on} (= k_{cat} + k_{off}/K_M) by ~30-fold (Table S1) and increased k_{off} by ~40-fold (k_{on} = 7.0 × 10^5 M^{-1} s^{-1}; k_{off} = 3.6 ± 0.9 × 10^{-3} s^{-1}; Figures S6A and S6B). The K_D value (5.2 nM) calculated from these k_{on} and k_{off} values agrees well with the K_D (2.3 ± 0.6 nM) measured by equilibrium competition experiments (Figure 4 and Table S4). Our data provide strong support for the idea that in flies seed pairing must precede the formation of base pairs between the target and the 3′ half of the siRNA.

Base Pairing Beyond the Seed Proceeds at a Slower Rate for Fly Ago2-RISC

In contrast, the calculated k_{on} (k_{on} = 2.4 × 10^7 M^{-1} s^{-1}) for fly Ago2-RISC binding a fully complementary target is ~10 times slower than for a seed-matching target. For fully complementary targets in flies, (k_{cat} + k_{off})/K_M approximates k_{on} and should reflect the rate at which RISC attains a catalytically active conformation, i.e., pairing from g2 to g17. Calculating k_{on} from enzyme kinetics yields a similar value: 5.9 × 10^7 M^{-1} s^{-1} (Figure 3E). Taken together, our data suggest that seed pairing occurs more rapidly than the subsequent propagation of base pairs across the center of the siRNA and through the 3′ supplementary region.

We imagine that complete base pairing to fully complementary targets requires conformational rearrangement of the siRNA within fly Ago2-RISC. Structural studies of eubacterial and eukaryotic Argonautes support this idea. They reveal a conformational rearrangement of the protein near the center of the guide when it is extensively paired to its target and release of its 3′ end from the PAZ domain of Argonaute (Wang et al., 2009; Boland et al., 2011). In this view, cleavage of a target by fly Ago2-RISC is not limited by the search for a complementary sequence among the RNAs in a cell but rather by the rate at which the siRNA, bound to Argonaute, can form an additional ~8 base pairs beyond the seed.

In contrast, mouse AGO2-RISC associates with a fully paired target at a rate (k_{on} = 3.6 × 10^7 M^{-1} s^{-1}) indistinguishable from seed (k_{on} = 2.0 × 10^7 M^{-1} s^{-1}) or seed plus 3′ supplementary pairing (k_{on} = 3.6 × 10^7 M^{-1} s^{-1}). The association rate derived from enzyme kinetics corroborates these measurements: k_{on} = (k_{off} + k_{cat})/K_M = 2.0 × 10^7 M^{-1} s^{-1} (Figure 6D). Thus, fly Ago2 binds rapidly through its seed, then completes pairing of its 3′ bases more slowly, whereas mouse AGO2 binds seed-matching targets more slowly, so that the rate of propagating the helix to the 3′ half of the guide does not limit the rate of target cleavage.

Centrally Bulged Sites

Centrally bulged siRNAs are often used to model miRNA function in cultured mammalian cells (Zeng et al., 2002; Doench and Sharp, 2004; Broderick et al., 2011). This approach typically uses an asymmetric 3 × 2 internal loop at g9–g11. Although we have not measured the binding of 3 × 2 asymmetric internal loops, our results with 3 × 3 symmetric internal loops are likely to be similar. Compared to naturally occurring, seed-match sites, centrally bulged sites bind RISC 80-fold more tightly for fly Ago2 (Figure 4), suggesting an explanation why centrally bulged sites require a lower concentration of RISC to mediate reporter repression (Broderick et al., 2011).

Although a target with g9–g11 mismatch bound fly Ago2-RISC as tightly as a fully complementary RNA (K_D = 3.0 ± 1.0 pM; Figure 4 and Table S4), the mechanism of binding is clearly different from the fully paired target: its measured k_{off} value of 1.1 ± 0.1 × 10^{-3} s^{-1} and calculated k_{on} value of 3.1 × 10^8 M^{-1} s^{-1} are 5- to 13-fold faster than the fully complementary target (Figures S6A and S6B). We propose that the g9–g11 mismatch bypasses an energetically unfavorable rearrangement that occurs for a fully complementary target RNA. Interestingly, the crystal structure of eubacterial Argonaute shows that both ends of the guide remain anchored in the presence of a g10g11 mismatch (Wang et al., 2008a).

DISCUSSION

Argonaute divides a small RNA guide into anchor, seed, central, 3′ supplementary, and tail functional domains (Figure 7). Nucleotides in the anchor (g1) and tail (g18–g21) facilitate Argonaute loading and help secure the siRNA or miRNA guide to Argonaute after the passenger or miRNA* strand has been removed. But these terminal domains are unlikely to base pair with a target RNA, even when pairing is predicted by their sequences. In contrast, central base pairing (g9–g12) between the guide and target is required for efficient target cleavage. Mismatches in this central region prevent RISC from attaining a catalytically competent conformation. For fly Ago2-RISC, achieving this conformation takes more time than seed pairing alone. Our data show that nearly every fly Ago2-RISC that reaches this conformation cleaves its RNA target rather than releasing it. For mouse AGO2-RISC, a slow catalytic rate often allows the target to escape before being sliced.

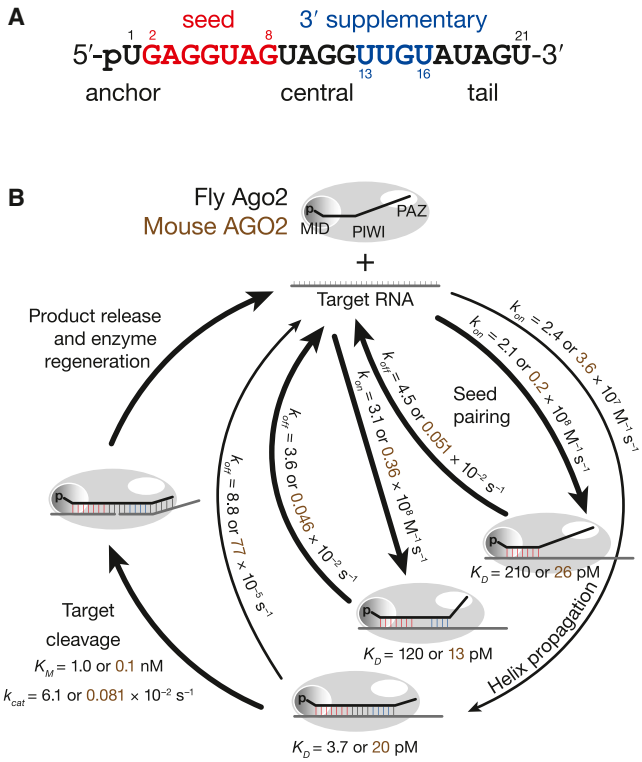

Figure 7. Model for RISC Function

(A) Loading of an siRNA or miRNA into Argonaute creates distinct functional domains in the RNA guide.

(B) A model for RISC binding and cleavage of target RNA. See also Figure S7.

In contrast, most miRNA:Argonaute complexes rapidly bind to and dissociate from their RNA targets via their seed. Even when RISC binds a target through both its seed and 3′ supplementary regions, it dissociates nearly as rapidly as for seed-only binding. Thus, the properties of RISC are essentially the same for both the typical seed-only and the less common seed plus 3′ supplementary pairing targets. That the rates of association and dissociation are so similar for these two binding modes suggests that pairing between a target and the 3′ supplementary region of a miRNA does not require winding the target RNA around the guide, side-stepping the topological problem that must be solved for siRNAs to direct RISC to cleave a target.

The finding that miRNAs use so little of their sequence to identify their regulatory targets surprised the biological community (Wightman et al., 1993; Lai and Posakony, 1998; Reinhart et al., 2000; Lai, 2002). Our data show that miRNA-programmed RISC binds with a strength and binding site size similar to those of high affinity RNA-binding proteins (e.g., Hall and Stump, 1992; Zamore et al., 1999; Zearfoss et al., 2011; Wright et al., 2011). It is siRNA-programmed RISC whose behavior should surprise us: it binds highly complementary targets far *less* tightly than a comparable antisense RNA because Argonaute reduces the contribution of most of its nucleotides to target binding.

What do the physical properties of RISC teach us about its cellular function? miRNAs and siRNAs are typically present in cells at dramatically different concentrations. For example, in flies in which the *white* gene is silenced by RNAi, the abundance of all antisense *white* siRNAs combined is less than that of any of 29 most abundant miRNAs (Ghildiyal et al., 2008). Previously, the ability of siRNAs to function at low abundance has been ascribed to the catalytic nature of RNAi (Fire et al., 1998; Montgomery et al., 1998; Hutvágner and Zamore, 2002). To achieve a concentration 10-fold greater than the K_D for siRNA-like binding (3.7 pM for fly Ago2-RISC) would require only ~5 molecules of RISC in ovarian terminal filament cells (~200 μm^3; Schneider, 1972) and ~11 molecules in a cultured S2 cell (~500 μm^3; Sarikaya et al., 2012). Thus, even for Argonaute proteins with no endonuclease activity, small numbers of molecules of RISC can repress highly complementary targets; endonuclease activity is only needed when a small amount of RISC must repress a larger amount of target. The combination of high affinity and catalytic turnover helps explain why the siRNA-directed RNAi pathway provides an effective defense against viral infection in plants and invertebrate animals (Hamilton and Baulcombe, 1999; Wilkins et al., 2005; Galiana-Arnoux et al., 2006; Wang et al., 2006).

Animal miRNAs nearly always repress their targets by binding rather than endonucleolytic cleavage. This explains why animal cells express miRNAs at such high levels. Recent data suggest that only the most abundant cellular miRNAs mediate target repression (Mullokandov et al., 2012). Our data provide a biochemical explanation for this observation.

Consider two abundant miRNAs in a cultured HeLa cell (~5,000 μm^3; Cohen and Studzinski, 1967; Milo et al., 2010): miR-21 (4 nM; Lim et al., 2003) and the *let-7* miRNA family, nine highly related miRNAs sharing a common seed sequence (~3 nM; Cole et al., 2009). Both miRNAs are present at a concentration greater than the K_D we measured for seed matched targets for fly (~210 pM) or mouse (~26 pM) Ago2-RISC. Assuming a mean target mRNA abundance of ten molecules per cell and 50 different mRNA targets per miRNA, miR-21 and *let-7* each regulate ~500 (170 pM) total target mRNA molecules per HeLa cell (Friedman et al., 2009). Under these conditions, nearly every miR-21 or *let-7* target mRNA (~95%–99%) with an accessible seed match will be bound by the complementary miRNA-programmed RISC (Figure S7).

Target repression by miRNAs can be reduced by the presence of competitor RNAs containing miRNA binding sites that titrate miRNA-RISC away from the mRNAs it regulates (Arvey et al., 2010; Garcia et al., 2011; Mukherji et al., 2011). The fundamental properties of RISC make specific predictions about how the activity of specific miRNAs can be inhibited by the expression of these competitor transcripts. The effect of such competitor RNAs reflects the concentration of both the miRNA and miRNA-binding sites (Ebert and Sharp, 2012), as well as the affinity of miRNA-RISC for those sites. For abundant miRNAs such as miR-21 or the *let-7* family, the expression of competitor RNAs containing miRNA binding sites—even highly complementary binding sites—will have little impact on the regulation of their target genes in flies or mammals. Doubling the expression of mRNAs repressed by miR-21, for example, would require ~7.8 nM seed only competitor and ~4.0 nM fully paired competitor for fly Ago2-RISC. For mouse AGO2-RISC, it would still require ~7.7 nM seed only competitor and ~7.2 nM of the fully paired competitor. Taken together, this translates to ~22,400

copies of seed only competitor and ~12,000–21,700 copies of fully paired competitor (Figure S7). If the competitor contained one miRNA-binding site, it would comprise 12%–50% of all the mRNA in the cell (Islam et al., 2011).

In contrast, doubling the expression of the mRNA targets for an intermediate (mir-93; ~140 pM) or a low abundance miRNA (mir-24; 7.3 pM) would require just 600–800 additional seed-matching sites (Figure S7). For mir-93 whose abundance confers the ability to bind to ~60% of all potential targets, the competitor must be as abundant as the sum of all the target mRNAs (~500 copies). Low abundance miRNAs like mir-24 are unlikely to contribute much biologically meaningful regulation because they are present at a concentration less than their K_D for seed-matching targets in both flies and mammals: <4% of miR-24 targets are expected to be bound by the miRNA at any given time. Using the conservative assumption that every bound miRNA-RISC completely represses an mRNA target, miR-24 is predicted to reduce the expression of the average seed-matched target by <4% (Figure S7).

Thus, the proposal that "competing endogenous RNAs" ("ceRNAs") sequester miRNAs, derepressing the authentic targets of that miRNA (Salmena et al., 2011), applies only to a small subset of miRNAs whose cellular concentration and target abundance meet a narrow range of values. The miRNAs with the largest impact on gene expression—the most abundant miRNAs—are not predicted to be regulatable by endogenous, transcribed seed-matched competitor transcripts. Consistent with this view, viral and experimental inhibition of specific miRNA function by transcribed RNA requires the use of extensively complementary miRNA-binding sites that recruit a cellular pathway that actively degrades the targeted miRNA (Ebert et al., 2007; Loya et al., 2009; Ameres et al., 2010; Xie et al., 2012). Absent this target directed, catalytic destruction of miRNAs, RNAs of ordinary abundance are unlikely to compete with mRNAs for binding abundant, biologically functional miRNAs.

EXPERIMENTAL PROCEDURES

General Methods

Target cleavage reactions were performed as described (Haley and Zamore, 2004; Haley et al., 2003) except with 4 mM Mg^{2+}. Cleavage targets (Table S2) were prepared by in vitro transcription and capping (Haley et al., 2003). For binding, synthetic RNAs were 5′ or 3′ ^{32}P radiolabeled.

Binding, Competition, and Dissociation Assays

Ago2-RISC was assembled with *let-7* siRNA in 0–2 hr embryo lysate or S100 from immortalized *Ago2*$^{-/-}$ MEFs expressing mouse AGO2 (O'Carroll et al., 2007). Binding reactions were at 25°C for 1 hr; protein-RNA complexes were captured on nitrocellulose and unbound RNA on Nylon membranes under vacuum and washed with ice-cold buffer. Competition reactions were at 25°C for 1 hr (mouse) or 6 hr (fly). For k_{off}, Ago2-RISC was incubated with ^{32}P-radiolabeled RNA target for 1 hr then competitor RNA was added and dissociation measured.

SUPPLEMENTAL INFORMATION

Supplemental Information includes Extended Experimental Procedures, seven figures, and four tables and can be found with this article online at http://dx.doi.org/10.1016/j.cell.2012.10.036.

ACKNOWLEDGMENTS

We thank D. Turner, J. Chen, A. Carruthers, R. Gilmore, S. Ryder, B. Farley, O. Bilsel, S. Kathuria, and P. Gandhi for help and discussions; the Turner lab for use of equipment; A. Boucher, T. Covello, and G. Farley for technical support; and members of the Zamore lab for critical comments on the manuscript. This work was supported in part by National Institutes of Health grants GM62862 and GM65236. Phillip D. Zamore is a cofounder and scientific advisor to Alnylam Pharmaceuticals.

Received: June 29, 2012
Revised: September 11, 2012
Accepted: October 8, 2012
Published: November 20, 2012

REFERENCES

Amarzguioui, M., Holen, T., Babaie, E., and Prydz, H. (2003). Tolerance for mutations and chemical modifications in a siRNA. Nucleic Acids Res. *31*, 589–595.

Ameres, S.L., Martinez, J., and Schroeder, R. (2007). Molecular basis for target RNA recognition and cleavage by human RISC. Cell *130*, 101–112.

Ameres, S.L., Horwich, M.D., Hung, J.H., Xu, J., Ghildiyal, M., Weng, Z., and Zamore, P.D. (2010). Target RNA-directed trimming and tailing of small silencing RNAs. Science *328*, 1534–1539.

Arvey, A., Larsson, E., Sander, C., Leslie, C.S., and Marks, D.S. (2010). Target mRNA abundance dilutes microRNA and siRNA activity. Mol. Syst. Biol. *6*, 363.

Bartel, D.P. (2009). MicroRNAs: target recognition and regulatory functions. Cell *136*, 215–233.

Berg, O.G., and von Hippel, P.H. (1985). Diffusion-controlled macromolecular interactions. Annu. Rev. Biophys. Biophys. Chem. *14*, 131–160.

Bhattacharyya, S.N., Habermacher, R., Martine, U., Closs, E.I., and Filipowicz, W. (2006). Relief of microRNA-mediated translational repression in human cells subjected to stress. Cell *125*, 1111–1124.

Boland, A., Huntzinger, E., Schmidt, S., Izaurralde, E., and Weichenrieder, O. (2011). Crystal structure of the MID-PIWI lobe of a eukaryotic Argonaute protein. Proc. Natl. Acad. Sci. USA *108*, 10466–10471.

Brennecke, J., Stark, A., Russell, R.B., and Cohen, S.M. (2005). Principles of microRNA-target recognition. PLoS Biol. *3*, e85.

Broderick, J.A., Salomon, W.E., Ryder, S.P., Aronin, N., and Zamore, P.D. (2011). Argonaute protein identity and pairing geometry determine cooperativity in mammalian RNA silencing. RNA *17*, 1858–1869.

Brown, K.M., Chu, C.Y., and Rana, T.M. (2005). Target accessibility dictates the potency of human RISC. Nat. Struct. Mol. Biol. *12*, 469–470.

Cohen, L.S., and Studzinski, G.P. (1967). Correlation between cell enlargement and nucleic acid and protein content of HeLa cells in unbalanced growth produced by inhibitors of DNA synthesis. J. Cell. Physiol. *69*, 331–339.

Cole, C., Sobala, A., Lu, C., Thatcher, S.R., Bowman, A., Brown, J.W., Green, P.J., Barton, G.J., and Hutvagner, G. (2009). Filtering of deep sequencing data reveals the existence of abundant Dicer-dependent small RNAs derived from tRNAs. RNA *15*, 2147–2160.

Ding, H., Schwarz, D.S., Keene, A., Affar, B., Fenton, L., Xia, X., Shi, Y., Zamore, P.D., and Xu, Z. (2003). Selective silencing by RNAi of a dominant allele that causes amyotrophic lateral sclerosis. Aging Cell *2*, 209–217.

Doench, J.G., and Sharp, P.A. (2004). Specificity of microRNA target selection in translational repression. Genes Dev. *18*, 504–511.

Ebert, M.S., and Sharp, P.A. (2012). Roles for microRNAs in conferring robustness to biological processes. Cell *149*, 515–524.

Ebert, M.S., Neilson, J.R., and Sharp, P.A. (2007). MicroRNA sponges: competitive inhibitors of small RNAs in mammalian cells. Nat. Methods *4*, 721–726.

Elbashir, S.M., Martinez, J., Patkaniowska, A., Lendeckel, W., and Tuschl, T. (2001). Functional anatomy of siRNAs for mediating efficient RNAi in *Drosophila melanogaster* embryo lysate. EMBO J. *20*, 6877–6888.

Elcheva, I., Goswami, S., Noubissi, F.K., and Spiegelman, V.S. (2009). CRD-BP protects the coding region of betaTrCP1 mRNA from miR-183-mediated degradation. Mol. Cell *35*, 240–246.

Elkayam, E., Kuhn, C.D., Tocilj, A., Haase, A.D., Greene, E.M., Hannon, G.J., and Joshua-Tor, L. (2012). The structure of human argonaute-2 in complex with miR-20a. Cell *150*, 100–110.

Fire, A., Xu, S., Montgomery, M.K., Kostas, S.A., Driver, S.E., and Mello, C.C. (1998). Potent and specific genetic interference by double-stranded RNA in *Caenorhabditis elegans*. Nature *391*, 806–811.

Friedman, R.C., Farh, K.K., Burge, C.B., and Bartel, D.P. (2009). Most mammalian mRNAs are conserved targets of microRNAs. Genome Res. *19*, 92–105.

Galiana-Arnoux, D., Dostert, C., Schneemann, A., Hoffmann, J.A., and Imler, J.L. (2006). Essential function in vivo for Dicer-2 in host defense against RNA viruses in *drosophila*. Nat. Immunol. *7*, 590–597.

Garcia, D.M., Baek, D., Shin, C., Bell, G.W., Grimson, A., and Bartel, D.P. (2011). Weak seed-pairing stability and high target-site abundance decrease the proficiency of *lsy-6* and other microRNAs. Nat. Struct. Mol. Biol. *18*, 1139–1146.

Ghildiyal, M., Seitz, H., Horwich, M.D., Li, C., Du, T., Lee, S., Xu, J., Kittler, E.L., Zapp, M.L., Weng, Z., and Zamore, P.D. (2008). Endogenous siRNAs derived from transposons and mRNAs in *Drosophila* somatic cells. Science *320*, 1077–1081.

Goswami, S., Tarapore, R.S., Teslaa, J.J., Grinblat, Y., Setaluri, V., and Spiegelman, V.S. (2010). MicroRNA-340-mediated degradation of microphthalmia-associated transcription factor mRNA is inhibited by the coding region determinant-binding protein. J. Biol. Chem. *285*, 20532–20540.

Grimson, A., Farh, K.K., Johnston, W.K., Garrett-Engele, P., Lim, L.P., and Bartel, D.P. (2007). MicroRNA targeting specificity in mammals: determinants beyond seed pairing. Mol. Cell *27*, 91–105.

Ha, I., Wightman, B., and Ruvkun, G. (1996). A bulged *lin-4*/*lin-14* RNA duplex is sufficient for *Caenorhabditis elegans lin-14* temporal gradient formation. Genes Dev. *10*, 3041–3050.

Haley, B., and Zamore, P.D. (2004). Kinetic analysis of the RNAi enzyme complex. Nat. Struct. Mol. Biol. *11*, 599–606.

Haley, B., Tang, G., and Zamore, P.D. (2003). In vitro analysis of RNA interference in *Drosophila melanogaster*. Methods *30*, 330–336.

Hall, K.B., and Stump, W.T. (1992). Interaction of N-terminal domain of U1A protein with an RNA stem/loop. Nucleic Acids Res. *20*, 4283–4290.

Hamilton, A.J., and Baulcombe, D.C. (1999). A species of small antisense RNA in posttranscriptional gene silencing in plants. Science *286*, 950–952.

Hammes, G.G., and Schimmel, P.R. (1970). 2 Rapid Reactions and Transient States. In Enzymes D, *Volume 2*, B. Paul, ed. (San Diego: Academic Press), pp. 67–114.

Holen, T., Amarzguioui, M., Wiiger, M.T., Babaie, E., and Prydz, H. (2002). Positional effects of short interfering RNAs targeting the human coagulation trigger Tissue Factor. Nucleic Acids Res. *30*, 1757–1766.

Huang, J., Liang, Z., Yang, B., Tian, H., Ma, J., and Zhang, H. (2007). Derepression of microRNA-mediated protein translation inhibition by apolipoprotein B mRNA-editing enzyme catalytic polypeptide-like 3G (APOBEC3G) and its family members. J. Biol. Chem. *282*, 33632–33640.

Hutvágner, G., and Zamore, P.D. (2002). A microRNA in a multiple-turnover RNAi enzyme complex. Science *297*, 2056–2060.

Islam, S., Kjällquist, U., Moliner, A., Zajac, P., Fan, J.B., Lönnerberg, P., and Linnarsson, S. (2011). Characterization of the single-cell transcriptional landscape by highly multiplex RNA-seq. Genome Res. *21*, 1160–1167.

Jafarifar, F., Yao, P., Eswarappa, S.M., and Fox, P.L. (2011). Repression of VEGFA by CA-rich element-binding microRNAs is modulated by hnRNP L. EMBO J. *30*, 1324–1334.

John, B., Enright, A.J., Aravin, A., Tuschl, T., Sander, C., and Marks, D.S. (2004). Human MicroRNA targets. PLoS Biol. *2*, e363.

Kawamata, T., Seitz, H., and Tomari, Y. (2009). Structural determinants of miRNAs for RISC loading and slicer-independent unwinding. Nat. Struct. Mol. Biol. *16*, 953–960.

Kedde, M., Strasser, M.J., Boldajipour, B., Oude Vrielink, J.A., Slanchev, K., le Sage, C., Nagel, R., Voorhoeve, P.M., van Duijse, J., Ørom, U.A., et al. (2007). RNA-binding protein Dnd1 inhibits microRNA access to target mRNA. Cell *131*, 1273–1286.

Kertesz, M., Iovino, N., Unnerstall, U., Gaul, U., and Segal, E. (2007). The role of site accessibility in microRNA target recognition. Nat. Genet. *39*, 1278–1284.

Krek, A., Grün, D., Poy, M.N., Wolf, R., Rosenberg, L., Epstein, E.J., MacMenamin, P., da Piedade, I., Gunsalus, K.C., Stoffel, M., and Rajewsky, N. (2005). Combinatorial microRNA target predictions. Nat. Genet. *37*, 495–500.

Lai, E.C. (2002). Micro RNAs are complementary to 3′ UTR sequence motifs that mediate negative post-transcriptional regulation. Nat. Genet. *30*, 363–364.

Lai, E.C., and Posakony, J.W. (1998). Regulation of *Drosophila* neurogenesis by RNA:RNA duplexes? Cell *93*, 1103–1104.

Lewis, B.P., Shih, I.H., Jones-Rhoades, M.W., Bartel, D.P., and Burge, C.B. (2003). Prediction of mammalian microRNA targets. Cell *115*, 787–798.

Lewis, B.P., Burge, C.B., and Bartel, D.P. (2005). Conserved seed pairing, often flanked by adenosines, indicates that thousands of human genes are microRNA targets. Cell *120*, 15–20.

Lim, L.P., Lau, N.C., Weinstein, E.G., Abdelhakim, A., Yekta, S., Rhoades, M.W., Burge, C.B., and Bartel, D.P. (2003). The microRNAs of *Caenorhabditis elegans*. Genes Dev. *17*, 991–1008.

Lim, L.P., Lau, N.C., Garrett-Engele, P., Grimson, A., Schelter, J.M., Castle, J., Bartel, D.P., Linsley, P.S., and Johnson, J.M. (2005). Microarray analysis shows that some microRNAs downregulate large numbers of target mRNAs. Nature *433*, 769–773.

Long, D., Lee, R., Williams, P., Chan, C.Y., Ambros, V., and Ding, Y. (2007). Potent effect of target structure on microRNA function. Nat. Struct. Mol. Biol. *14*, 287–294.

Loya, C.M., Lu, C.S., Van Vactor, D., and Fulga, T.A. (2009). Transgenic microRNA inhibition with spatiotemporal specificity in intact organisms. Nat. Methods *6*, 897–903.

Ma, J.B., Yuan, Y.R., Meister, G., Pei, Y., Tuschl, T., and Patel, D.J. (2005). Structural basis for 5′-end-specific recognition of guide RNA by the *A. fulgidus* Piwi protein. Nature *434*, 666–670.

Martinez, J., and Tuschl, T. (2004). RISC is a 5′ phosphomonoester-producing RNA endonuclease. Genes Dev. *18*, 975–980.

Milo, R., Jorgensen, P., Moran, U., Weber, G., and Springer, M. (2010). BioNumbers—the database of key numbers in molecular and cell biology. Nucleic Acids Res. *38*(Database issue), D750–D753.

Miranda, K.C., Huynh, T., Tay, Y., Ang, Y.S., Tam, W.L., Thomson, A.M., Lim, B., and Rigoutsos, I. (2006). A pattern-based method for the identification of MicroRNA binding sites and their corresponding heteroduplexes. Cell *126*, 1203–1217.

Montgomery, M.K., Xu, S., and Fire, A. (1998). RNA as a target of double-stranded RNA-mediated genetic interference in *Caenorhabditis elegans*. Proc. Natl. Acad. Sci. USA *95*, 15502–15507.

Mukherji, S., Ebert, M.S., Zheng, G.X., Tsang, J.S., Sharp, P.A., and van Oudenaarden, A. (2011). MicroRNAs can generate thresholds in target gene expression. Nat. Genet. *43*, 854–859.

Mullokandov, G., Baccarini, A., Ruzo, A., Jayaprakash, A.D., Tung, N., Israelow, B., Evans, M.J., Sachidanandam, R., and Brown, B.D. (2012). High-throughput assessment of microRNA activity and function using microRNA sensor and decoy libraries. Nat. Methods *9*, 840–846.

Nakanishi, K., Weinberg, D.E., Bartel, D.P., and Patel, D.J. (2012). Structure of yeast Argonaute with guide RNA. Nature *486*, 368–374.

O'Carroll, D., Mecklenbrauker, I., Das, P.P., Santana, A., Koenig, U., Enright, A.J., Miska, E.A., and Tarakhovsky, A. (2007). A Slicer-independent role for Argonaute 2 in hematopoiesis and the microRNA pathway. Genes Dev. *21*, 1999–2004.

Parker, J.S., Roe, S.M., and Barford, D. (2005). Structural insights into mRNA recognition from a PIWI domain-siRNA guide complex. Nature *434*, 663–666.

Parker, J.S., Parizotto, E.A., Wang, M., Roe, S.M., and Barford, D. (2009). Enhancement of the seed-target recognition step in RNA silencing by a PIWI/MID domain protein. Mol. Cell *33*, 204–214.

Reinhart, B.J., Slack, F.J., Basson, M., Pasquinelli, A.E., Bettinger, J.C., Rougvie, A.E., Horvitz, H.R., and Ruvkun, G. (2000). The 21-nucleotide *let-7* RNA regulates developmental timing in *Caenorhabditis elegans*. Nature *403*, 901–906.

Rivas, F.V., Tolia, N.H., Song, J.J., Aragon, J.P., Liu, J., Hannon, G.J., and Joshua-Tor, L. (2005). Purified Argonaute2 and an siRNA form recombinant human RISC. Nat. Struct. Mol. Biol. *12*, 340–349.

Salmena, L., Poliseno, L., Tay, Y., Kats, L., and Pandolfi, P.P. (2011). A ceRNA hypothesis: the Rosetta Stone of a hidden RNA language? Cell *146*, 353–358.

Sarikaya, D.P., Belay, A.A., Ahuja, A., Dorta, A., Green, D.A., 2nd, and Extavour, C.G. (2012). The roles of cell size and cell number in determining ovariole number in *Drosophila*. Dev. Biol. *363*, 279–289.

Schirle, N.T., and MacRae, I.J. (2012). The crystal structure of human Argonaute2. Science *336*, 1037–1040.

Schneider, I. (1972). Cell lines derived from late embryonic stages of *Drosophila melanogaster*. J. Embryol. Exp. Morphol. *27*, 353–365.

Schroeder, S.J., and Turner, D.H. (2009). Optical melting measurements of nucleic acid thermodynamics. Methods Enzymol. *468*, 371–387.

Schwarz, D.S., Ding, H., Kennington, L., Moore, J.T., Schelter, J., Burchard, J., Linsley, P.S., Aronin, N., Xu, Z., and Zamore, P.D. (2006). Designing siRNA that distinguish between genes that differ by a single nucleotide. PLoS Genet. *2*, e140.

Song, J.J., Smith, S.K., Hannon, G.J., and Joshua-Tor, L. (2004). Crystal structure of Argonaute and its implications for RISC slicer activity. Science *305*, 1434–1437.

Tafer, H., Ameres, S.L., Obernosterer, G., Gebeshuber, C.A., Schroeder, R., Martinez, J., and Hofacker, I.L. (2008). The impact of target site accessibility on the design of effective siRNAs. Nat. Biotechnol. *26*, 578–583.

Takeda, Y., Mishima, Y., Fujiwara, T., Sakamoto, H., and Inoue, K. (2009). DAZL relieves miRNA-mediated repression of germline mRNAs by controlling poly(A) tail length in zebrafish. PLoS ONE *4*, e7513.

Tang, G., Reinhart, B.J., Bartel, D.P., and Zamore, P.D. (2003). A biochemical framework for RNA silencing in plants. Genes Dev. *17*, 49–63.

Toledano, H., D'Alterio, C., Czech, B., Levine, E., and Jones, D.L. (2012). The let-7-Imp axis regulates ageing of the *Drosophila* testis stem-cell niche. Nature *485*, 605–610.

Tomari, Y., Du, T., and Zamore, P.D. (2007). Sorting of *Drosophila* small silencing RNAs. Cell *130*, 299–308.

Wang, X.H., Aliyari, R., Li, W.X., Li, H.W., Kim, K., Carthew, R., Atkinson, P., and Ding, S.W. (2006). RNA interference directs innate immunity against viruses in adult *Drosophila*. Science *312*, 452–454.

Wang, Y., Juranek, S., Li, H., Sheng, G., Tuschl, T., and Patel, D.J. (2008a). Structure of an argonaute silencing complex with a seed-containing guide DNA and target RNA duplex. Nature *456*, 921–926.

Wang, Y., Sheng, G., Juranek, S., Tuschl, T., and Patel, D.J. (2008b). Structure of the guide-strand-containing argonaute silencing complex. Nature *456*, 209–213.

Wang, Y., Juranek, S., Li, H., Sheng, G., Wardle, G.S., Tuschl, T., and Patel, D.J. (2009). Nucleation, propagation and cleavage of target RNAs in Ago silencing complexes. Nature *461*, 754–761.

Wightman, B., Ha, I., and Ruvkun, G. (1993). Posttranscriptional regulation of the heterochronic gene *lin-14* by *lin-4* mediates temporal pattern formation in *C. elegans*. Cell *75*, 855–862.

Wilkins, C., Dishongh, R., Moore, S.C., Whitt, M.A., Chow, M., and Machaca, K. (2005). RNA interference is an antiviral defence mechanism in *Caenorhabditis elegans*. Nature *436*, 1044–1047.

Wright, J.E., Gaidatzis, D., Senften, M., Farley, B.M., Westhof, E., Ryder, S.P., and Ciosk, R. (2011). A quantitative RNA code for mRNA target selection by the germline fate determinant GLD-1. EMBO J. *30*, 533–545.

Xia, T., SantaLucia, J.J., Jr., Burkard, M.E., Kierzek, R., Schroeder, S.J., Jiao, X., Cox, C., and Turner, D.H. (1998). Thermodynamic parameters for an expanded nearest-neighbor model for formation of RNA duplexes with Watson-Crick base pairs. Biochemistry *37*, 14719–14735.

Xie, J., Ameres, S.L., Friedline, R., Hung, J.H., Zhang, Y., Xie, Q., Zhong, L., Su, Q., He, R., Li, M., et al. (2012). Long-term, efficient inhibition of microRNA function in mice using rAAV vectors. Nat. Methods *9*, 403–409.

Yekta, S., Shih, I.H., and Bartel, D.P. (2004). MicroRNA-directed cleavage of HOXB8 mRNA. Science *304*, 594–596.

Yoda, M., Kawamata, T., Paroo, Z., Ye, X., Iwasaki, S., Liu, Q., and Tomari, Y. (2010). ATP-dependent human RISC assembly pathways. Nat. Struct. Mol. Biol. *17*, 17–23.

Yuan, Y.R., Pei, Y., Ma, J.B., Kuryavyi, V., Zhadina, M., Meister, G., Chen, H.Y., Dauter, Z., Tuschl, T., and Patel, D.J. (2005). Crystal structure of *A. aeolicus* argonaute, a site-specific DNA-guided endoribonuclease, provides insights into RISC-mediated mRNA cleavage. Mol. Cell *19*, 405–419.

Zamore, P.D., Bartel, D.P., Lehmann, R., and Williamson, J.R. (1999). The PUMILIO-RNA interaction: a single RNA-binding domain monomer recognizes a bipartite target sequence. Biochemistry *38*, 596–604.

Zearfoss, N.R., Clingman, C.C., Farley, B.M., McCoig, L.M., and Ryder, S.P. (2011). Quaking regulates Hnrnpa1 expression through its 3′ UTR in oligodendrocyte precursor cells. PLoS Genet. *7*, e1001269.

Zeng, Y., Wagner, E.J., and Cullen, B.R. (2002). Both natural and designed micro RNAs can inhibit the expression of cognate mRNAs when expressed in human cells. Mol. Cell *9*, 1327–1333.

EXTENDED EXPERIMENTAL PROCEDURES

Kinetics

Target cleavage reactions were performed as described (Haley and Zamore, 2004; Haley et al., 2003) except with 4 mM Mg^{2+}. For each siRNA duplex, guide position 1 (g1) was unpaired from the corresponding base in the passenger strand to ensure efficient loading of the guide strand into Ago2 (Schwarz et al., 2003; Khvorova et al., 2003; Förstemann et al., 2007; Tomari et al., 2007). *let-7* is not present in the *Drosophila* embryo lysate used in our studies. For multiple-turnover reactions, 20 nM siRNA duplex was incubated with 0–2 hr *Drosophila* embryo lysate at 25°C for 3 min to assemble fly Ago2-RISC; for single-turnover reactions, 50 nM siRNA duplex was incubated with embryo lysate for 90 min to assemble more fly Ago2-RISC (Haley and Zamore, 2004). Subsequently, Ago2 assembly was inactivated by cooling the reaction to 4°C for 3 min and adding 1.0 mM (f.c.) *N*-ethylmaleimide (NEM). After 10 min, 1.2 mM (f.c.) DTT was added to quench unreacted NEM. RISC concentration was adjusted by dilution in NEM-treated embryo lysate (Haley et al., 2003). Control experiments demonstrated that target cleavage required Ago2. Single-turnover reactions employed 0.1, 0.5 or 1 nM (f.c.) target RNA. Pre-steady-state experiments were performed in 100 mM potassium acetate, 18 mM HEPES (pH 7.4), 3 mM magnesium acetate, 5 mM DTT, 0.01% (v/v) IGEPAL CA-630, 0.01 mg/ml baker's yeast tRNA with 100 nM substrate (f.c) at 25°C. For each time point, an aliquot of the reaction was quenched in 200 mM Tris-HCl (pH 7.5), 25 mM EDTA (pH 8.0), 300 mM NaCl, 2% (w/v) sodium dodecyl sulfate, 2 μg/μl Proteinase K and 0.2 μg/μl glycogen carrier. All samples were resolved by urea-denaturing polyacrylamide gel electrophoresis (Haley et al., 2003). Gels were dried, exposed to image plates, and then scanned and analyzed with an FLA-5000 or FLA9000 (GE Healthcare Bioscience, Pittsburgh, PA) and Image Gauge 4.22 software (Fujifilm, Tokyo).

siRNAs and Target RNAs

Synthetic siRNA duplexes (Dharmacon, ThermoFisher Scientific, Lafayette, CO; Sigma-Aldrich Corp, St. Louis, MO) were deprotected, phosphorylated and gel purified (Table S2). RNA targets (Table S2) were prepared by in vitro capping and transcription (Haley et al., 2003). Briefly, DNA transcription templates were generated by PCR (Table S2) from pGL2-Control vector (Promega, Madison, WI). RNA was transcribed with T7 RNA polymerase and gel purified. Next, 150 pmol RNA was incubated for 1.5 hr at 37°C in a 40 μl reaction containing 1.25 μM ^{32}P α-GTP (Perkin Elmer, Waltham, MA), 25 U guanylyl transferase (Epicenter, Madison, WI), 40 U RNase inhibitor (Promega, Madison, WI), 125 μM *S*-adenosylmethionine, 50 mM Tris-HCl (pH 8.0), 6 mM KCl and 1.25 mM $MgCl_2$. Next, 15 U guanylyl transferase, 1.2 mM GTP, a concentration in excess of the RNA substrate and greater than the K_M of the enzyme (Myette and Niles, 1996), 120 μM *S*-adenosylmethionine were added and incubation continued for 1.5 hr. Capped RNA was gel purified, and small aliquots were frozen in liquid nitrogen and stored at −80°C. Target RNAs were radiolabeled with 0.1 mM [5′-^{32}P] cytidine-3′,5′-bisphosphate, 0.5 U/μl T4 RNA ligase (Ambion, Life Technologies, Grand Island, NY), 0.3 U/μl SUPERase•In (Ambion) 10% (v/v) dimethylsulfoxide at 4°C overnight. RNA was gel purified and concentration determined by absorbance at 260 nm.

Measurement of ΔG of Base Pairing by Hyperchromicity Analysis

RNA hyperchromicity analyses were performed in 100 mM KCl, 18 mM sodium cacodylate (pH 7.4) and 4 mM $MgCl_2$. Equimolar amounts of the two RNAs were used for each duplex. Control experiments established that none of the individual RNA strands contained stable intramolecular structure. Absorbance at 260 nm was measured every 0.5°C from 10°C to 80°C at a heating rate of 1°C min^{-1} with a DU 640 spectrophotometer with a high performance temperature controller (Beckman Coulter, Indianapolis, IN). Data were fit to a two-state model with Meltwin (McDowell and Turner, 1996; Schroeder and Turner, 2009).

Nearest Neighbor Analysis

$\Delta G_{25°C} = -RT \ln(1/K_M)$, where R = 1.987 cal $K^{-1}mol^{-1}$ and T = 298.15K. Error was propagated with the quadratic sum of the partial uncertainties (Taylor, 1997). Theoretical $\Delta G_{25°C}$ was calculated based on nearest neighbors values and with RNAstructure 5.3 (Xia et al., 1998; Reuter and Mathews, 2010). The seed was taken to correspond to g2–g8, and 3′ supplementary pairing to correspond to g12–g17.

Binding, Competition, and Dissociation Assays

Fly Ago2-RISC was assembled for 90 min with *let-7* siRNA (5′-pUGA GGU AGU AGG UUG UAU AGU-3′) with 0–2 hr embryo lysate. Mouse AGO2-RISC was assembled for 90 min with *let-7* siRNA with S100 extract. The S100 extract was obtained from *Ago2*$^{-/-}$ mouse embryonic fibroblasts (MEFs) immortalized with SV40 large T-antigen that stably overexpressed mouse AGO2 (O'Carroll et al., 2007). Briefly, MEF cells were grown to confluence in 5% CO_2 at 37°C in DMEM (Invitrogen, Life Technologies) supplemented with 15% fetal bovine serum (PAA Laboratories, Inc., Dartmouth, MA) and 50 U/ml penicillin and streptomycin (Invitrogen, Life Technologies). S100 extract was prepared as described (Dignam et al., 1983) except that the cell pellet was washed three times in ice-cold PBS and once in buffer A that contains 10 mM HEPES–KOH (pH 7.9), 10 mM potassium acetate, 1.5 mM magnesium acetate, 0.5 mM DTT and EDTA-free protease inhibitor cocktail. Then, the pellet is resuspended in twice its volume with buffer A and incubated on ice for 20 min. This allows the cells to swell and subsequently lysed (with 20 strokes) with a Dounce homogenizer and a tight pestle (B type) on ice. The homogenate was centrifuged gently at 2,000 × *g* to remove nuclei and cell membranes. Next, 0.11 volume (that of the clarified supernatant from the low speed centrifugation) of buffer that consists of 300 mM HEPES-KOH

(pH 7.9), 1.4 M potassium acetate, 30 mM magnesium acetate, 0.5 mM DTT and EDTA-free protease inhibitor cocktail was added. This was immediately followed by ultracentrifugation at 100,000 × *g* at 4°C for 20 min where the supernatant constitutes the S100 extract. Ice-cold 80% (w/v) glycerol is then added to the S100 extract to achieve a 13% (w/v) final glycerol concentration. Finally, the S100 extract was, aliquoted, frozen in liquid nitrogen, and stored at −80°C. The protein concentration of the S100 extract was ~3–4 mg/ml. Assembled Ago2-RISC was captured with a 5′ biotinylated 2′-*O*-methyl-modified oligonucleotide that pairs with g2–g8 and g13–g16 of *let-7* seed (5′-Biotin-AUA GAC UGC GAC AAU AGC CUA CCU CCG AAC G-3′) and eluted with a DNA oligonucleotide bearing four 2′-*O*-methyl modifications (m); 5′-GGmU AmGG CTA TmUmG TCG CAG TCT AT-3′ (C.F.F.-J. and P.D.Z., unpublished data). Fly Ago2-RISC eluate was further purified with Superdex 200 HR 10/300 GL (GE Healthcare Bioscience, Pittsburgh, PA) size exclusion column. Mouse AGO2-RISC eluate was subsequently purified with Mono S 5/50 GL (GE Healthcare) cationic exchanger. Column purified fly Ago2-RISC was concentrated by centrifugation (3,000 × *g*; Amicon Ultra-0.5 ml, Millipore, Billerica, MA) in 100 mM potassium acetate, 18 mM HEPES (pH 7.4), 3 mM magnesium acetate, 5 mM DTT, 0.01% (v/v) IGEPAL CA-630, 0.01 mg/ml baker's yeast tRNA (equilibration buffer). Column purified mouse AGO2-RISC was dialyzed with a 3 ml *Slide-A-Lyzer* cassette (Pierce, ThermoFisher Scientific) in equilibration buffer supplemented to a final concentration of 20% glycerol (v/v). Finally, mouse AGO2-RISC is concentrated by centrifugation. Binding reactions were incubated at 25°C for 1 hr. RNA binding was measured by capturing protein-RNA complexes on Protran nitrocellulose membrane (Whatman, GE Healthcare Bioscience, Pittsburgh, PA) and unbound RNA on a Nylon XL membrane (GE Healthcare Bioscience) with a Bio-Dot apparatus (Bio-Rad, Hercules, CA). After applying the sample under vacuum, membranes were washed with ice-cold equilibration buffer. Membranes were air-dried and signals detected by phosphorimaging. Competition reactions were incubated at 25°C for 1 (mouse AGO2-RISC) or 6 hr (fly Ago2-RISC). To measure dissociation rate constants, 0.5–5 nM Ago2-RISC was incubated with 0.5 nM ^{32}P-radiolabeled RNA target for 1 hr, then 50 nM or 500 nM competitor RNA was added and dissociation measured by filter binding.

Measuring the Concentration of Purified Ago2-RISC

RNA guide was extracted from Ago2-RISC and resolved along with concentration standards by 15% denaturing polyacrylamide gel electrophoresis. RNA was transferred from the gel to Hybond-NX membrane (Amersham Biosciences, Piscataway, NJ) at 20 V for 1 hr, cross-linked to the membrane with 1-ethyl-3-(3-dimethylaminopropyl) carbodiimide (Pall and Hamilton, 2008), and probed as described to detect the guide and standards (Table S2A; Ameres et al., 2010; Han et al., 2011).

Data Analysis and Kinetic Modeling

When [E] << [S], time courses were fit to y = mx + b; when [S] < [E], time courses were fit to $y = y_0 + Ae^{-kx}$, where the initial rate, $v_0 = Ak$ (Lu and Fei, 2003). Initial rates measured at different substrate concentrations were fit to the Michaelis-Menten model with Visual Enzymics 2008 (Softzymics, Princeton, NJ) for Igor Pro 6.11,

$$v = \frac{V_{\max}[S_T]}{K_M + [S_T]}$$

or to the Morrison quadratic equation for tight binding,

$$v = V_{\max}\frac{([S_T] + [E_T] + K_M) - \sqrt{([S_T] + [E_T] + K_M)^2 - 4[E_T][S_T]}}{2[E_T]}$$

with Igor Pro 6.11 (WaveMetrics, Lake Oswego, OR). The rate of product formation was determined separately for each replicate, and significance determined with Student's two-tailed, two-sample, equal variance t test (Excel, Microsoft, Seattle, WA). R 2.14.0 software was used for other statistical analyses. To obtain the enzyme concentration by pre-steady-state analysis, data were fit with nonlinear least square regression in Igor Pro 6 to the burst and steady state equation,

$$F(t) = E \times \frac{a^2}{(a+b)^2}\left(1 - e^{-(a+b)t}\right) + E \times \frac{ab}{(a+b)}t$$

where *F(t)* is target cleaved with time, *E* is the enzyme concentration, *a* and *b* are rate constants according to the following scheme,

$$E + S \xrightarrow{a} EI \xrightarrow{b} E + P$$

Because K_D < [RNA target], all binding data were fit to

$$f = \frac{([E_T] + [S_T] + K_D) - \sqrt{([E_T] + [S_T] + K_D)^2 - 4([E_T][S_T])}}{2[S_T]}$$

where *f* is fraction target bound, $[E_T]$ is total enzyme concentration, $[S_T]$ is total RNA target concentration, and K_D is the apparent equilibrium dissociation constant.

For competition assays, the apparent equilibrium dissociation constant, K_C, for the competitor RNAs was obtained by fitting the data to the normalized quadratic solution of the Lin and Riggs equation (Lin and Riggs, 1972; Weeks and Crothers, 1992),

$$\Theta = \frac{\left([E_T] + [S_T] + K_D + \frac{K_D[C_T]}{K_C}\right) - \sqrt{\left([E_T] + [S_T] + K_D + \frac{K_D[C_T]}{K_C}\right)^2 - 4([E_T][S_T])}}{2[S_T]}$$

where Θ is the fraction target bound in the presence of competitor RNA, $[C_T]$, with an apparent dissociation constant of K_C. To obtain the dissociation rate constant, k_{off}, data were fit to $f = e^{-k_{off}t}$; $t_{½} = \ln(2)/k_{off}$.

Berkeley Madonna 8.3.18 (www.berkeleymadonna.com/index.html) was used to model target derepression of miRNA-RISC by target competitors for high (human miR-21), intermediate (human miR-93) and low (human miR-24) abundance miRNAs. The concentration of miR-21 RISC (4 nM) was calculated with the reported abundance of ~12,000 copies per HeLa cell, assuming a maximum cell volume of 5,000 μm^3 (Lim et al., 2003; Moran et al., 2010). The concentrations of miRNA-RISC for miR-93 and miR-24 were calculated, relative to miR-21, based on published ratios of sequencing reads (Cole et al., 2009).

SUPPLEMENTAL REFERENCES

Ameres, S.L., Horwich, M.D., Hung, J.H., Xu, J., Ghildiyal, M., Weng, Z., and Zamore, P.D. (2010). Target RNA-directed trimming and tailing of small silencing RNAs. Science *328*, 1534–1539.

Cole, C., Sobala, A., Lu, C., Thatcher, S.R., Bowman, A., Brown, J.W., Green, P.J., Barton, G.J., and Hutvagner, G. (2009). Filtering of deep sequencing data reveals the existence of abundant Dicer-dependent small RNAs derived from tRNAs. RNA *15*, 2147–2160.

Dignam, J.D., Lebovitz, R.M., and Roeder, R.G. (1983). Accurate transcription initiation by RNA polymerase II in a soluble extract from isolated mammalian nuclei. Nucleic Acids Res. *11*, 1475–1489.

Förstemann, K., Horwich, M.D., Wee, L., Tomari, Y., and Zamore, P.D. (2007). *Drosophila* microRNAs are sorted into functionally distinct argonaute complexes after production by dicer-1. Cell *130*, 287–297.

Haley, B., and Zamore, P.D. (2004). Kinetic analysis of the RNAi enzyme complex. Nat. Struct. Mol. Biol. *11*, 599–606.

Haley, B., Tang, G., and Zamore, P.D. (2003). In vitro analysis of RNA interference in *Drosophila melanogaster*. Methods *30*, 330–336.

Han, B.W., Hung, J.H., Weng, Z., Zamore, P.D., and Ameres, S.L. (2011). The 3′-to-5′ exoribonuclease Nibbler shapes the 3′ ends of microRNAs bound to Drosophila Argonaute1. Curr. Biol. *21*, 1878–1887.

Khvorova, A., Reynolds, A., and Jayasena, S.D. (2003). Functional siRNAs and miRNAs exhibit strand bias. Cell *115*, 209–216.

Lim, L.P., Lau, N.C., Weinstein, E.G., Abdelhakim, A., Yekta, S., Rhoades, M.W., Burge, C.B., and Bartel, D.P. (2003). The microRNAs of *Caenorhabditis elegans*. Genes Dev. *17*, 991–1008.

Lin, S.Y., and Riggs, A.D. (1972). Lac repressor binding to non-operator DNA: detailed studies and a comparison of eequilibrium and rate competition methods. J. Mol. Biol. *72*, 671–690.

Lu, W.P., and Fei, L. (2003). A logarithmic approximation to initial rates of enzyme reactions. Anal. Biochem. *316*, 58–65.

McDowell, J.A., Turner, D.H. (1996) Investigation of the structural basis for thermodynamic stabilities of tandem GU mismatches: solution structure of (rGAGGUCUC)2 by two-dimensional NMR and simulated annealing. Biochemistry *35*, 14077–14089.

Moran, U., Phillips, R., and Milo, R. (2010). SnapShot: key numbers in biology. Cell *141*, 1262-1262.e1.

Myette, J.R., and Niles, E.G. (1996). Domain structure of the vaccinia virus mRNA capping enzyme. Expression in Escherichia coli of a subdomain possessing the RNA 5′-triphosphatase and guanylyltransferase activities and a kinetic comparison to the full-size enzyme. J. Biol. Chem. *271*, 11936–11944.

O'Carroll, D., Mecklenbrauker, I., Das, P.P., Santana, A., Koenig, U., Enright, A.J., Miska, E.A., and Tarakhovsky, A. (2007). A Slicer-independent role for Argonaute 2 in hematopoiesis and the microRNA pathway. Genes Dev. *21*, 1999–2004.

Pall, G.S., and Hamilton, A.J. (2008). Improved northern blot method for enhanced detection of small RNA. Nat. Protoc. *3*, 1077–1084.

Reuter, J.S., and Mathews, D.H. (2010). RNAstructure: software for RNA secondary structure prediction and analysis. BMC Bioinformatics *11*, 129.

Schroeder, S.J., and Turner, D.H. (2009). Optical melting measurements of nucleic acid thermodynamics. Methods Enzymol. *468*, 371–387.

Schwarz, D.S., Hutvágner, G., Du, T., Xu, Z., Aronin, N., and Zamore, P.D. (2003). Asymmetry in the assembly of the RNAi enzyme complex. Cell *115*, 199–208.

Taylor, J.R. (1997). An Introduction to Error Analysis: The Study of Uncertainties in Physical Measurements (Sausalito, Calif.: University Science Books).

Tomari, Y., Du, T., and Zamore, P.D. (2007). Sorting of *Drosophila* small silencing RNAs. Cell *130*, 299–308.

Weeks, K.M., and Crothers, D.M. (1992). RNA binding assays for Tat-derived peptides: implications for specificity. Biochemistry *31*, 10281–10287.

Xia, T., SantaLucia, J.J., Jr., Burkard, M.E., Kierzek, R., Schroeder, S.J., Jiao, X., Cox, C., and Turner, D.H. (1998). Thermodynamic parameters for an expanded nearest-neighbor model for formation of RNA duplexes with Watson-Crick base pairs. Biochemistry *37*, 14719–14735.

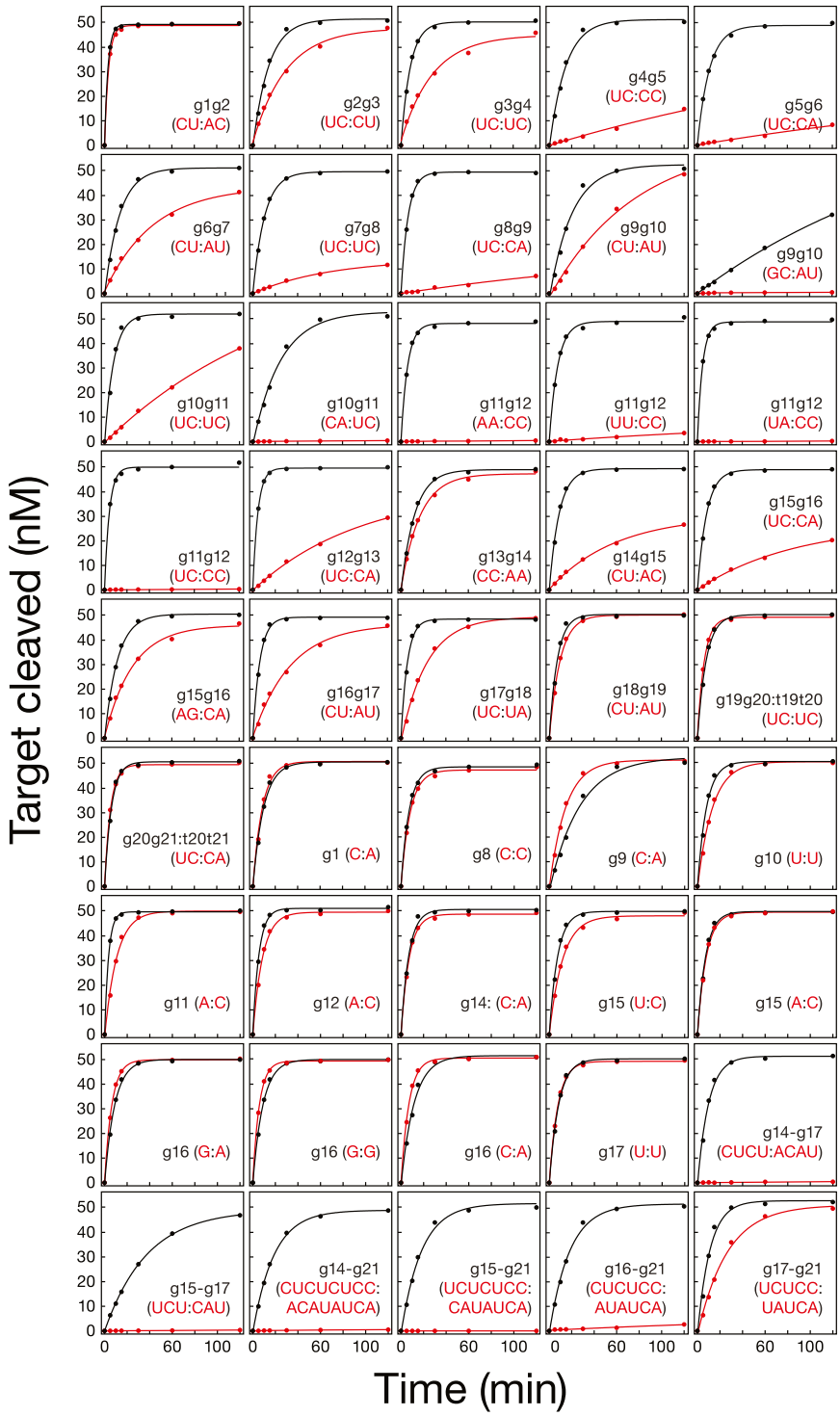

Figure S1. Target Cleavage by *let-7*-Programmed Fly Ago2-RISC, Related to Figure 1

Red, mismatched targets; Black, fully complementary. Substrate was in excess over enzyme (S = 50 nM, E ~3 nM).

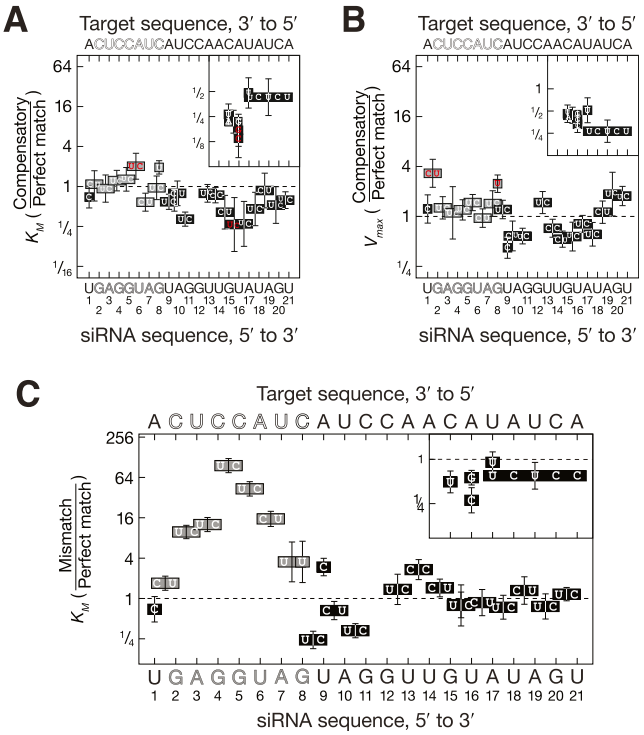

Figure S2. Michaelis-Menten Kinetics of Fly Ago2-RISC with Compensatory Targets, Related to Figure 1

(A) Relative K_M for fly Ago2-RISC comparing the individual fully complementary targets for all the *let-7* derivatives to the original fully complementary target for the parental *let-7* siRNA guide. Values that differed significantly (p value < 0.05) from the parental *let-7* target are highlighted in red.

(B) As in (A) but for relative V_{max}.

(C) Values for the K_M of mismatched *let-7* variant siRNAs relative to the K_M of the parental *let-7* for its fully complementary target RNA.

Values are reported as mean ± standard deviation for three independent experiments.

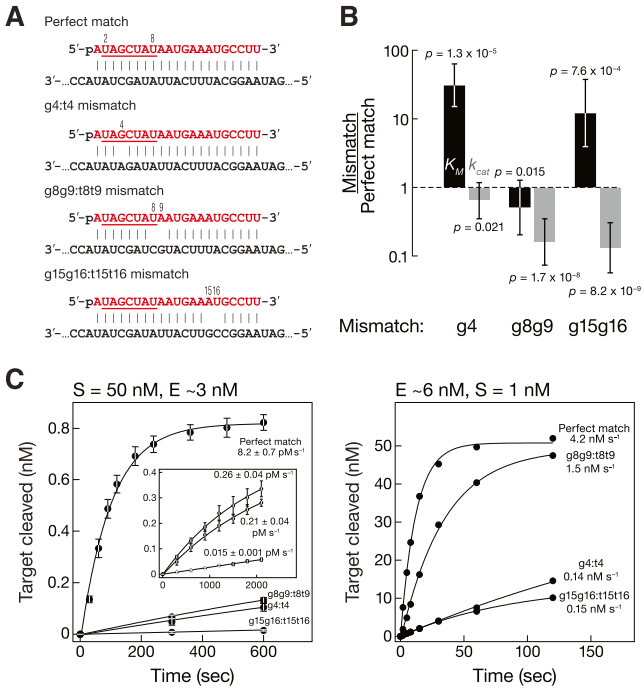

Figure S3. Fly Ago2-RISC Loaded With *Luciferase* siRNA, Related to Figure 1

(A) Scheme for a *Renilla reniformis* luciferase siRNA (red) pairing with its targets.

(B) Michaelis-Menten parameters for *luciferase* siRNA for mismatched targets, relative to the corresponding fully complementary target RNA. Mean K_M and k_{cat} values (±standard deviation) are from eight independent experiments. p values calculated with two-tailed Student's t test.

(C) Target cleavage by fly Ago2-RISC loaded with *luciferase* siRNA with enzyme (left) and substrate excess (right). Initial rates are reported to the right of each curve. Data represent mean ± standard deviation for four independent experiments.

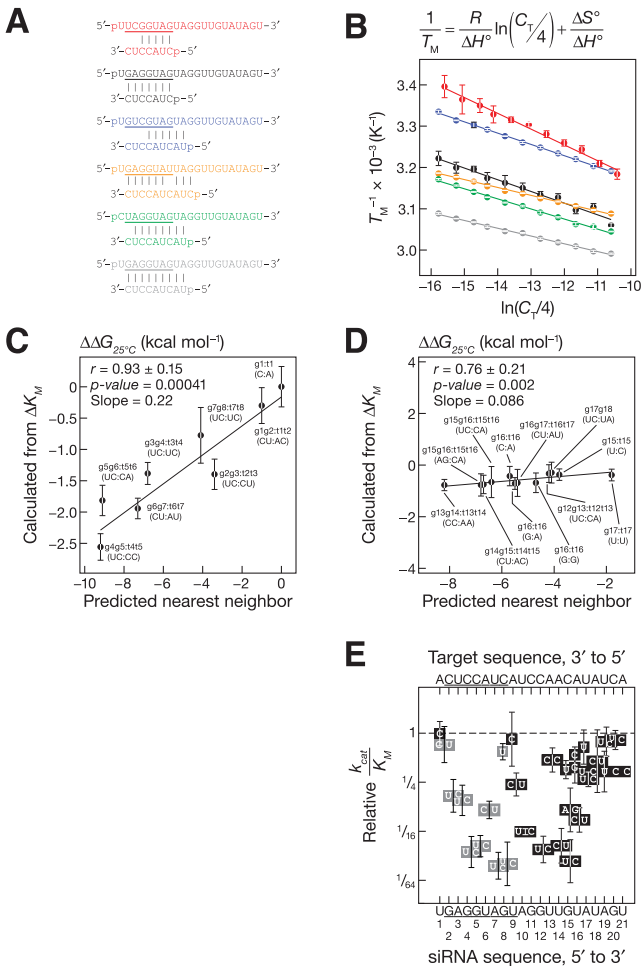

Figure S4. Base Pairing in Fly Ago2-RISC Obeys the Standard Rules for RNA, Related to Figure 3

(A) RNA duplexes used to measure the effect of mismatches on the strength of base pairing under standard RNAi reaction conditions.

(B) Van't Hoff plots for the RNA duplexes in (A). C_T is the total single-strand RNA concentration.

(C and D) Comparison of the $\Delta\Delta G_{25^\circ C}$ derived from K_M and the $\Delta\Delta G_{25^\circ C}$ calculated by nearest neighbor analysis between fully complementary targets and targets with mismatches in the seed, positions g2–g8 (C) and in the g12–g18 region (D).

(E) Change in k_{cat}/K_M for all mismatches introduced into the *let-7* siRNA guide.

Values are mean ± standard deviation.

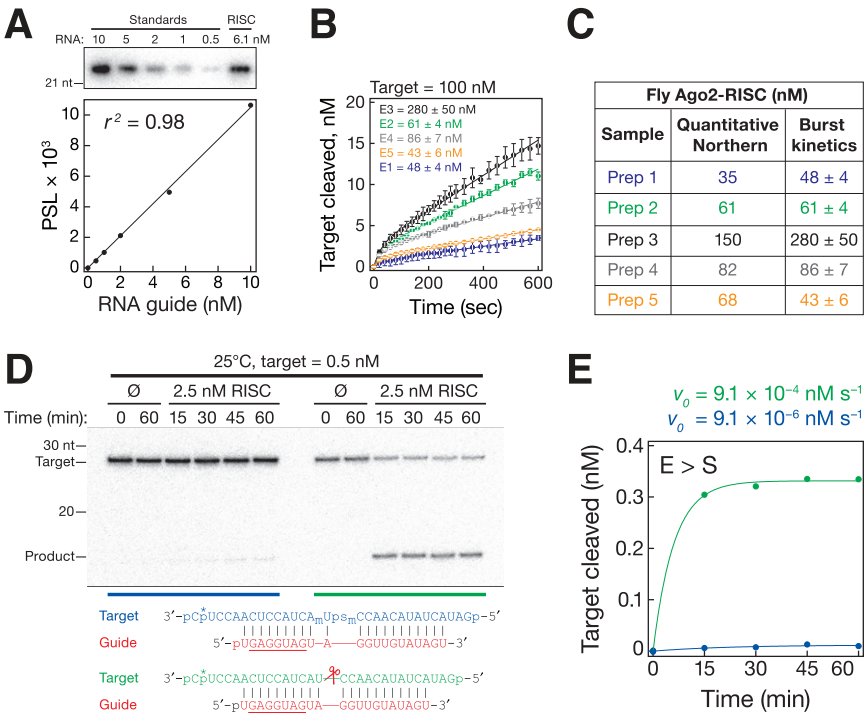

Figure S5. Purified Fly Ago2-RISC Binds a Fully Complementary Target RNA Tightly and Specifically, Related to Figure 3

(A) Quantitative northern hybridization to detect the *let-7* siRNA guide strand present in purified fly Ago2-RISC and to detect the corresponding *let-7* RNA concentration standards. Above, the gel image quantified to yield the graph below. PSL (background subtracted) are the units reported by the phosphorimager.

(B) Pre-steady-state "burst" kinetics to determine the amount of active *let-7* RISC present in five independent preparations of purified fly Ago2-RISC. Values are mean ± standard deviation.

(C) Concentrations of fly Ago2-RISC obtained by quantitative northern hybridization and pre-steady-state kinetics for the five independent preparations in (A) and (B).

(D) Time course of cleavage by fly Ago2-RISC with modified (blue) and unmodified (green) target RNA. A subscript "m" denotes 2′-*O*-methyl ribose; "ps" indicates a phosphorothioate linkage.

(E) Cleaved target (product) generated with time for the reactions shown in (D).

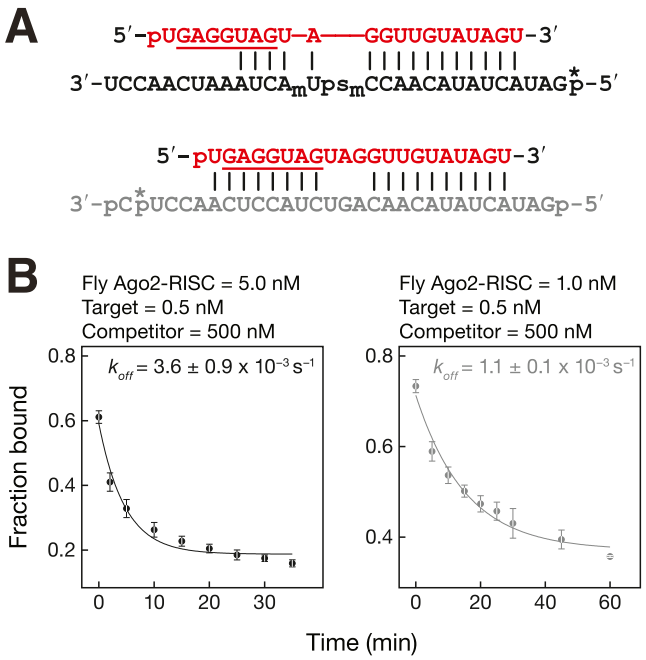

Figure S6. Mismatches Promote Target Dissociation, Related to Figure 5

(A) Target RNA bearing a g4g5:t4t5 mismatch (black) or g9–g11:t9–t11 mismatch (gray). An asterisk indicates the position of the ^{32}P-radiolabel; the subscript "m" indicates 2′-*O*-methyl ribose; "ps" indicates a phosphorothioate linkage.

(B) Dissociation rate curves for the targets shown in (A).

Data represent mean ± standard deviation for three independent experiments.

A

$$E + S \underset{k_{1r}}{\overset{k_{1f}}{\rightleftharpoons}} ES \qquad d(ES)/dt = k_{1f} \times (E_T - ES - EC) \times (S_T - ES) - (k_{1r} \times ES)$$

$$E + C \underset{k_{2r}}{\overset{k_{2f}}{\rightleftharpoons}} EC \qquad d(EC)/dt = k_{2f} \times (E_T - ES - EC) \times (C_T - EC) - (k_{2r} \times EC)$$

E = Free miRNA-RISC, E_T = Total miRNA-RISC
S = Free target, S_T = Total target = 0.17 nM
C = Free competitor, C_T = Total competitor
ES = miRNA-RISC:target complex
EC = miRNA-RISC:competitor complex

	fly Ago2	mouse AGO2
$k_{1f} = k_{2f} =$	0.21 nM^{-1} s^{-1}	0.020 nM^{-1} s^{-1}
$k_{1r} = k_{2r} =$	0.045 s^{-1}	5.0 x 10^{-4} s^{-1}
$k_{2f} =$	0.024 nM^{-1} s^{-1}	0.036 nM^{-1} s^{-1}
$k_{2r} =$	8.8 x 10^{-5} s^{-1}	7.7 x 10^{-4} s^{-1}

B

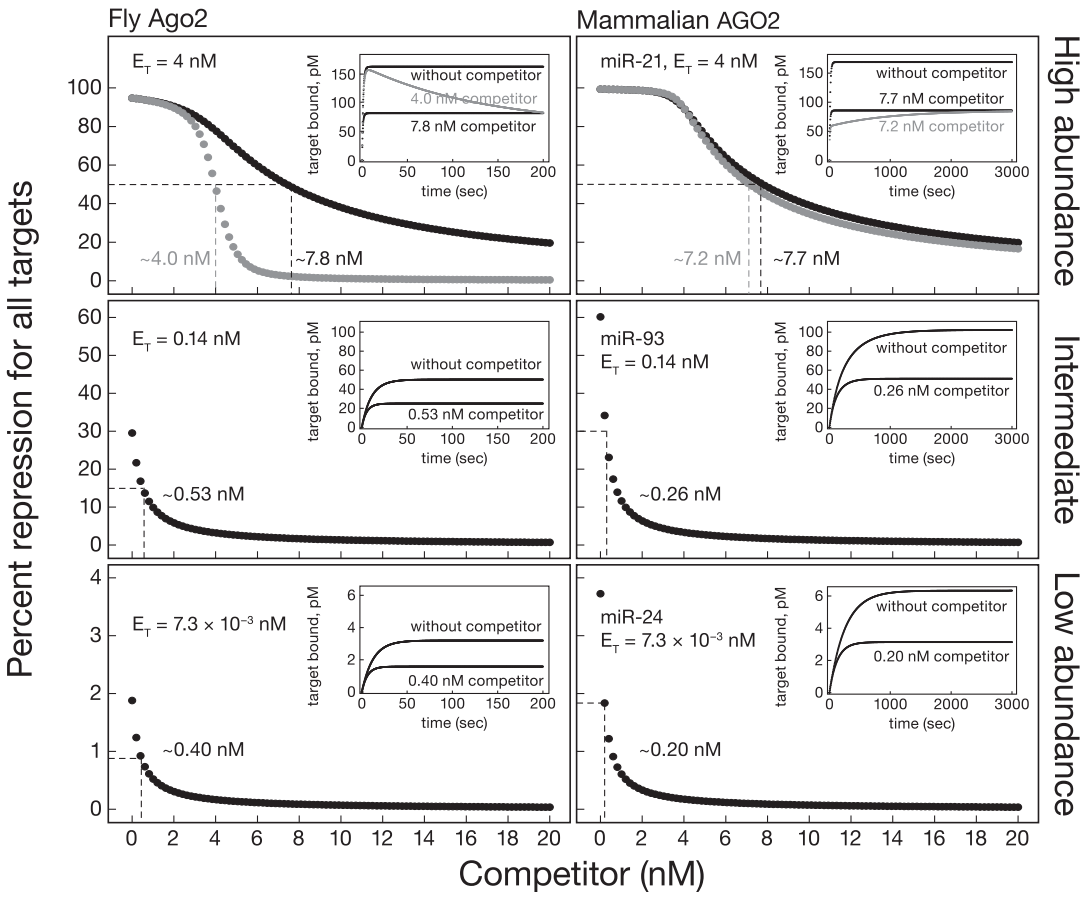

Figure S7. Modeling Target Tepression by miRNA, Related to Figure 7

(A) Reaction equations and rates.

(B) Predicted seed match or fully complementary (gray) competitor concentrations required to relieve 50% of repression by Ago2-RISC. Simulations used the k_{on} and k_{off} values measured for fly (left panels) or mouse AGO2 (right panels). We assume every bound miRNA-RISC fully represses its target. Insets show concentration of target bound with and without competitor.